Dynamic intestinal stem cell and mucosal remodeling by a mouse diet uniquely relevant to human risk and tumorigenesis

Short title: Stem Cells and Lineages in Tumor Risk

Jiahn Choi[1, ¶], Xusheng Zhang[2, ¶], Wenge Li[1, ¶], Michele Houston[1], Karina Peregrina[1], Robert Dubin[2], Kenny Ye[3], and Leonard H. Augenlicht[1,4, *]

[1] Department of Cell Biology, [2]Genetics, [3]Epidemiology and Population Health, [4]Medicine
Albert Einstein College of Medicine, Bronx, NY

[¶]These authors contributed equally

Acknowledgements: Supported in part by R01CA229216, R01CA214625, R01CA222358 and P30CA013330 from the NCI, NIH, USPHS.

***Corresponding Author**
Leonard H. Augenlicht
Professor, Department of Medicine and Cell Biology
Albert Einstein College of Medicine
Ullmann 909
1300 Morris Park Ave.
Bronx, NY 10461

Tel: 718 430-4247
Fax: 718 839-7925
laugenli@montefiore.org

All authors state there are no conflicts of interest

Posted as a pre-print on BioRxiv (*since revised*):
https://doi.org/10.1101/2022.03.17.484800

Data accession numbers: NCBI Gene Expression Omnibus (GEO) database: GSE186811; GSE188339; GSE188577; GSE188338.

Word Count text: 5733

Transparency: bulk and single cell RNAseq data sets are available from the public repositories; reagents will be made available to other investigators upon request to the corresponding author.

Synopsis: Mouse nutrient exposures uniquely reflecting those in humans dynamically remodel mouse stem cells and lineages, uniquely causing sporadic intestinal and colon tumors as in humans. Pathogenic mucosal alterations parallel aspects of human inflammatory bowel disease and plasticity of stem cell populations in human tumors.

Key words: Diet; tumor risk; stem cells; homeostasis; epigenetic reprogramming

Abstract

Background and Aims: NWD1 is a purified rodent diet unique in establishing mouse exposure to key nutrients recapitulating levels in the human that increase risk for intestinal cancer and supporting its unique relevance, NWD1 is the only rodent diet that causes sporadic intestinal and colon tumors in the mouse. The aim was to understand mechanisms of the dietary remodeling of stem cells and the mucosa in establishing the higher risk phenotype; **Methods:** Deconvolution of complex reprogramming and remodeling was by bulk and scRNAseq, scATACseq, functional genomics and imaging. **Results:** NWD1 extensively, rapidly, and reversibly reprogrammed Lgr5^{hi} stem cells, with epigenetic down-regulated *Ppargc1a* expression altering mitochondrial structure and function, suppressing Oxphos and the TCA cycle. This suppressed Lgr5^{hi} stem cell functions and developmental maturation of Lgr5^{hi} cell progeny as cells progressed through progenitor cell compartments. Mobilized *Bmi1+, Ascl2^{hi}* cells adapted lineages to the nutritional environment and elevated pathways of antigen processing and presentation, especially in mature enterocytes, leading to chronic low-level inflammation. **Conclusions:** Aspects of the reprogramming and remodeling of stem cells and mucosa parallel pathogenic mechanisms in human inflammatory bowel disease, also pro-tumorigenic, and the adaptive mucosal response determining which stem cells function is similar to recent data that human colon tumors are comprised of both Lgr5 positive and negative stem cells with the balance determined by the environment. Stem cell and mucosal plasticity in response to nutrient intake supports historic concepts of homeostasis as a continual process of tissue adaptation to its environment, with the human mucosa therefore likely in constant flux. Moreover, although oncogenic mutations provide a competitive advantage to intestinal stem cells in tumorigenesis, the competition takes place on a playing field sculpted by the nutritional environment, with a major influence on which cells dominate in mucosal maintenance and tumorigenesis.

Introduction:

The major influence of dietary patterns on risk for sporadic colon cancer [1], accounting for >70% of the human disease, has generated considerable interest in how nutrients alter intestinal stem cells and mucosal homeostasis. Investigations usually alter one or two nutrients in commonly used mouse diets to investigate reprogramming that may influence risk [2-5]. However, it has been emphasized that dietary patterns, not single nutrients, drive human risk [6-8], and we reported that effects of key nutrient exposures strongly linked to human risk for colon cancer are highly contextual, with the reprogramming of Lgr^{hi} stem cells very different depending on levels of other nutrients [9]. This is not surprising, since, for example, strongly penetrant onco- and tumor suppressor genes have vastly different effects in different tissues. This is of concern since almost all studies on nutrient remodeling of stem cells and the mucosa in the mouse common diets that establish exposure levels to key nutrients unrelated to levels actually present in humans. Thus, a logical premise is that to understand human risk, it is important to reflect human nutrient exposures, no different than that mouse genetic mutations and circuits should reflect those of the human and in pharmacological studies, drugs need to reflect levels relevant to those in humans.

A clear example that it is not only desirable, but essential, to better reflect human nutrient exposures to understand human physiology and pathogenesis is the key role of vitamin D in stem cell functions. The vitamin D receptor (Vdr) is one of 30 core genes in the 500 gene $Lgr5^{hi}$ stem cell signature, its expression robust in $Lgr5^{hi}$ cells, but immediately down-regulated in their daughter cells as they as they leave the stem cell niche and no longer function as stem cells [10]. *A priori***,** this suggests Vdr signaling is required for $Lgr5^{hi}$ stem cell functions, as well-established for hair follicle stem cells in both the mouse and human [11]. We showed this experimentally: a western diet (NWD1), including lower vitamin D_3 to reflect level strongly linked to human risk for colon tumors, suppressed $Lgr5^{hi}$ cell lineage tracing and efficiency in tumor

initiation, and more specifically, the lineage tracing was suppressed by Vdr genetic inactivation targeted to Lgr5 cells [9, 12, 13]. This is fundamental, since commonly used mouse diets establish vitamin D levels reflecting 0% of the population: 200-300% higher than population mean**,** 500% higher than levels linked to higher risk for CRC, and 25-50% higher than the highest level in only 1% of the population (reviewed in [9, 12-14]). Thus, common mouse diets create a nutritional environment supporting cell stem cell functions of Lgr5^{hi} cells, but at levels of a key nutrient unrelated to those in humans by orders of magnitude. This may contribute to mouse crypt base stem cells reaching crypt clonality 50 times faster than do these cells in humans (6 weeks vs 6 years, respectively), indeed suggested to be due to differences in nutritional environments [15-17]. Therefore, adjusting other nutrients may have interesting effects on stem cells and homeostasis, but this can be different, or short-circuited entirely, if stem cell functions are repressed by attenuated *Vdr* signaling, or altered by level of other nutrients not reflecting human exposures. The potential that this can may have an impact on relevance of the results to the human is independent of the subsequent experimental approach or rigor of the data generated.

These issues have rarely translated to design in stem cell investigations in the mouse, in part due to the major challenge presented by the complexity and variability of the human diet, with different valid ideas regarding how to better approach this for mice. Here we use the purified new western style diet 1 (NWD1) for two compelling reasons. NWD1 is formulated on the principal of nutrient density [18] to reflect mouse exposure to multiple key nutrients each at its level linked to elevated risk for colon cancer in broad segments of the population [18, 19]. Most important, in better reflecting actual human exposure to combined dietary risk factors, NWD1 is the only diet which causes mouse small and large intestinal sporadic tumors, uniquely reflecting the etiology, incidence, frequency and lag with developmental age of >70% of the human disease [19-22]. Therefore, it is striking that in NWD1 fed mice, the complexity of cellular and molecular alterations of stem cells and the mucosa altering risk differs markedly from that in

other models which do not reflect human nutrient exposures and in which sporadic tumors do not reproducibly arise.

Here bulk and single cell (sc)RNAseq, scATACseq, functional genomics and other methods de-convolve NWD1 remodeling of stem cells and lineages. NWD1 rapidly and reversibly reprogrammed stem cell metabolism by down-regulating *Ppargc1a*, altering mitochondrial structure and function that represses Lgr5^{hi} cell lineage tracing and developmental maturation of progeny cells as they progress through progenitor cell compartments. Alternate cells are mobilized to maintain the mucosa, adapting lineages to the altered nutritional environment and also dramatically elevating a pathway of antigen processing and presentation, especially in mature enterocytes, underlying development of chronic pro-tumorigenic inflammation. Importantly, specific elements of the NWD1 response parallel pathogenic mechanisms in the mucosa in human inflammatory bowel disease (IBD), which is also pro-tumorigenic [23, 24].

The novel results with NWD1 establish that dietary elevation of risk involves dynamic and complex remodeling of stem, progenitor and lineage differentiated cells early in the mucosa, a complexity of alteration documented in the uninvolved as well as involved mucosa of human IBD [23], and for the very earliest benign human tumors [25]. There is an overall adaptive response that includes determining which cells function as stem cells, similar to a recent finding that the environment provides selective pressure for whether Lgr5 positive or negative which stem cells dominate in mouse and human tumors [26]. Therefore, while oncogenic mutations provide a stem cell with a competitive advantage to expand in favoring tumor development [17], this competition is carried out on a playing field sculpted and continually remodeled by the nutritional environment, with a major effect on outcome.

Results:

NWD1 Impact on Lgr5^{hi} cells: Feeding NWD1 accelerates and amplifies tumorigenesis in multiple mouse models of intestinal cancer regardless of single or multiple genetic drivers [27-31], and in wild-type mice causes sporadic tumors [20, 22, 32].

Bulk RNAseq analyzed Lgr5^{hi} cells from *Lgr5$^{EGFP\text{-}creER}$* mice fed NWD1 or AIN76A control diet for 3 or 12 months from weaning (**Fig1A**: Arms 1, 2), or 3 months NWD1 then switched to AIN76A and sacrificed at 12 months (Arm 3 – crossover). >95% of Lgr5^{hi} stem cell signature genes [10] were down-regulated at 12 versus 3 months, regardless of diet (**Fig 1B,C**), the down-regulation persisting to at least 2 years of age [33]. For the broader Lgr5^{hi} cell transcriptome (~8,000 genes), NWD1 elevated and decreased expression of 164 and 63 genes, respectively, at 3 months, increasing 4-fold at 12 months to 551 and 229 and reverted to much more limited perturbation by dietary cross-over (**Fig 1D**). Thus, NWD1 had a major impact on reprogramming Lgr5^{hi} stem cells.

By gene set enrichment analysis (GSEA), NWD1 up- and down- regulated 25 and 30 pathways, respectively, in the Lgr5^{hi} cells at 3 months, many alterations persisting to 12 months of feeding, and reversed upon shift back to control AIN76A diet (**Table S1**). Oxphos and the TCA cycle are necessary for intestinal *Lgr5^{hi}* cells, hematopoietic, and embryonic cells to function as stem cells [34-38]. NWD1 significantly down-regulated these pathways at 3 months, persisting to 12 months of feeding, but was reversed by 12 months after switching mice back to control AIN76A at 3 months (**Fig 2, Table S1)**. 58 of 132 genes in the Oxphos pathway were down-regulated by NWD1 at 3 months, confirmed by interrogation of data from an independent cohort of mice also fed NWD1 or control AIN76A for 3 months ([9], **Fig 3A**). Mean decreased level of Oxphos gene expression was 14% and 11% in the two data sets (**Fig 3A**)**,** highly statistically significant, and persisted at 12 months. This encompassed multiple genes encoding subunits of the mitochondrial electron transport chain (**Fig 3C),** which were decreased by a mean of 10% (**Fig 3D;** $P=10^{-26}$, Fisher's exact test in comparison to the 8,000 member expressed gene set). Greatest down regulation in both cohorts were *Cox6a2* and *Cox7a1* of

cytochrome oxidase, the terminal respiratory chain enzyme, and *Sdhb*, and *Sdhd* of complex II, succinic dehydrogenase (**Fig 3B**) which are down-regulated in CRC and other cancers causing succinate accumulation and tumor development [39, 40]. In crossover to control diet (Arm 3), 52 (82%) of down-regulated Oxphos genes increased towards control levels, also highly significant (**Fig 3D;** $P=10^{-18}$), reflecting GSEA reversal (**Fig 2)**.

Thus, metabolic reprogramming of Lgr5^{hi} cells by NWD1 was prominent and dynamic, and a potential mechanism by which NWD1 suppressed Lgr5^{hi} stem cell functions [9, 12, 13]. In probing this more deeply, we noted *Ppargc1a* exhibited major alterations in response to diet. *Ppargc1a* encodes Pgc1a, a master regulator of metabolism and mitochondrial biogenesis [41, 42] and *Ppargc1a* overexpression elevates mitochondrial biogenesis and function of colonic epithelial cells, altering their fate [43]. NWD1 significantly reduced Lgr5^{hi} cell *Ppargc1a* expression by ≥60% in both mouse cohorts (**Fig 4A,C**), persisting to 12 months and reversed by dietary crossover (**Fig 4B**). NWD1 down-regulated Pgc1a protein was restricted to crypt base cells, with lower expression further up the villi that was not altered by diet (**Fig 4D,E**), confirmed by no detectable alteration in *Ppargc1a* expression in isolated Bmi1+ cells throughout the mucosa, determined by bulk RNAseq (**Fig 4F)**. This was paralleled by decreased mitochondria cristae density in crypt base columnar cells (**Fig 4H**), but no change in cristae density in crypt Paneth or in villus cells (**Fig 4H)**. Lgr5^{hi} GFP marked cells decreased by 60% in NWD1 mice (*P=0.03*, **Fig 4I)** and staining of FACS isolated Lgr5^{hi} GFP cells with Mitotracker red, an index of mitochondrial membrane potential and hence function, decreased in Lgr5^{hi} cells (*P<0.0001*; **Fig 4J**).

Mechanistic role of *Ppargc1a* down regulation: *Ppargc1a* was inactivated hetero- or homozygously in Lgr5^{hi} cells of mice fed control diet (*Lgr5*$^{EGFP\text{-}cre:ER\text{-}}$, *Ppargc1a*$^{loxp/loxp\ or\ loxp/+}$, *Rosa26*^{tom} mice). 3 days after homozygous *Ppargc1a* inactivation, effects of feeding NWD1 were phenocopied: Lgr5+ cell lineage tracing was suppressed (**Fig 5A,B,** *P=0.02*), and CBC cell cristae density decreased with no alteration in Paneth or in villus cells (**Fig 4G,H**).

To define how this mechanistically remodels the stem cells and the mucosa, scRNAseq analyzed FACs isolated intestinal epithelial cells (Epcam+, CD45neg) from mice 3 days after Lgr5 cell *Ppargc1a* inactivation. Twenty cell clusters aligned with intestinal cell types and all lineages (**Fig 5C**). A minor cluster could not be aligned (UK; <1% of cells in any single cell library). Cell proportion in each cluster was similar for all genotypes, but with increased early enterocyte populations (EC1 and EC2) at 5 days of heterozygous inactivation, that increased further and was statistically significant with homozygous inactivation (**Fig 5D**). Trajectory analysis placed EC1 proximal to Dividing cells, with EC2 emerging on that trajectory, and other EC cells and lineages arising further down-stream (**Fig 6A-C**). This predicted trajectory was validated by interrogating markers that identify physical cell position along the crypt-villus axis (**Fig 6F,** [44]). Therefore, altered EC1 and 2 cell number proximal to progenitor cells was consistent with the short 5 days between *Ppargc1a* genetic inactivation and scRNAseq analysis.

Repressed mitochondrial function suppresses ability of Lgr5^{hi} cells to function as stem cells [34-38], but mitochondrial function also can shift the balance between stem cells retaining self-renewal capacity or differentiating [45]. Therefore, progression of immature cells along the validated trajectory was investigated. At branch point “a”, developmental trajectory from the Replicating 1 cell compartment (R1) bifurcates to secretory goblet cell lineages or R2 cells (red arrow, **Fig 6A-C**). For both WT and *Ppargc1a* het mice, R1 cells were the major cell type at branch point “a” with few or no Stem cells (**Fig 6D**). Thus, at this early branch point, developmental transition from Stem to R1 had taken place. However, with homozygous *Ppargc1a* inactivation, 100% of cells at “a” were Stem cells, a major, and highly significant, repression of the re-programming with maturation from Stem to R1 cells (**Fig 6D**; $P=10^{-5}$, by a weighted linear regression based on cell number at each cluster for each mouse). This altered cell distribution at branch “a” with homozygous inactivation was paralleled by significant suppression of Oxphos, TCA cycle, cell cycle, and glycolysis pathways (**Fig 6D**). The highly

significant decrease in the Oxphos and TCA cycle pathways reflects the altered mitochondrial structure and function with *Ppargc1a* homozygous inactivation (**Fig 4G,H**).

With further cell maturation along the validated trajectory, branch point "b" was transition from R2 to enteroendocrine and Tuft cells (**Fig 6A-C**). At "b", most cells in WT or het mice had progressed to R2, but with homozygous *Ppargc1a* inactivation, 90% remained in R1 (*P=0.016*), with highly significant repression of the Oxphos pathway persisting (**Fig 6E**). Therefore, homozygous *Ppargc1a* inactivation altered Stem cell maturation to R1 cells, and repressed transition out of R1 with down-regulation of the Oxphos pathway, and a parallel enrichment in the glycolytic pathway.

Rapidity of dietary alterations: scRNAseq analyzed intestinal epithelial cells of mice fed AIN76A for 3 months (**Fig 7A**, Arm 1), these mice switched to NWD1 for 4 days (Arm 2), and the 4d NWD1 mice switched back again to AIN76A for 4 days (Arm 3). Stem, replicating, dividing cells and all lineages were identified**,** with no significant changes in cell distribution for clusters among the 3 arms (**Fig 7B,C**). As above, developmental progression of the clusters as they progressed through progenitor and lineage differentiation along the crypt-luminal axis was confirmed by expression of markers that physically identify cell position along this axis [44] (**Fig 7D**). For the stem cell cluster, 4 days of NWD1 altered 30 pathways with high significance ($P=10^{-3}$ *to* 10^{-45}) including repression (negative Z-score) of the TCA cycle and Oxphos (**Fig 8A,B**). 19 of the 30 pathways reverted to control values in 4d NWD1 mice switched back to AIN76A for 4 days. This included the TCA cycle: 8 genes encoding TCA cycle enzymes were down-regulated by 4d NWD1 switch and reversed by 4d switch-back to AIN76A (**Fig 8C**), reflecting the highly significant GSEA for dietary shifts (**Fig 8A,B**). However, while 4d of NWD1 decreased expression of 51 Oxphos pathway genes, reflecting the significant negative enrichment, only 15 of these reversed on switch back to AIN76A, and the lack of significant reversal for this pathway(**Fig 8B,C,D**). Therefore, within 4 days of shift to NWD1, stem cells at

the crypt base underwent significant metabolic re-programming, in large part, but not entirely, reversed within 4 days of shift back to control diet.

NWD1 mobilization of Bmi1+ cells: NWD1 expands the mouse intestinal proliferative cell compartment [46, 47], recapitulating expansion in humans at elevated CRC risk [48-51]. This suggests cells above the crypt base are mobilized as part of the adaptive response to the high risk diet, and we reported NWD1 induces lineage tracing from Bmi1+ positive cells above the crypt base, persisting for months as long as the mice remain on the western diet [9, 13]. Moreover, in targeting *Apc* inactivation to Bmi1+ cells, tumor development was increased when the mice were fed NWD1, paralleling acquisition of their ability to lineage trace in NWD1 fed mice [9, 12].

Acquisition of stem cell functions by dedifferentiation of cells above the crypt base following loss of Lgr5^{hi} stem cell function is well documented [17, 52]. To dissect dietary impact on Bmi1+ cells, scRNAseq data were generated for Bmi1+ marked cells and their marked epithelial cell progeny isolated from *Bmi1*$^{cre\text{-}ERT2}$*, Rosa26*^{tom} mice fed diets for 3 months from weaning (Tom+, Epcam+, CD45neg), at 3 days after Tam injection (shorter), or after marked cells had accumulated for 66-70 days (longer) (**Fig 9A,B**)**.** Stem, replicating, dividing, and all cell lineages were identified (**Fig 9C,D**), with similar cell cluster distributions among cell types regardless of diet (**Fig 9D**). Therefore, despite NWD1 repressing Lgr5^{hi} stem cell functions, the mucosa was maintained. As above, the predicted developmental trajectory of Bmi1+ cells was confirmed by expression of markers that identify cells at different positions along the crypt-luminal axis [44] (**Fig 9E**)

Expression of the stem cell transcription factor Ascl2 is a key driver of dedifferentiation of Bmi1+ cells to replace damaged Lgr5^{hi} cells [17, 52]. Regardless of diet or time post Bmi1+ cell marking, *Ascl2* gene expression characterized Stem1 and 2, Replicating and Dividing cells in trajectory analysis of the data (**Fig 10A,** blue arrows, quantified in **Fig 10B.** A small number of

Tuft and goblet cells also expressed *Ascl2* where goblet and enteroendocrine lineages diverged (**Fig 10A,** orange arrows, and **Fig 10B**).

Among the 4 progenitor cell compartments, *Ascl2* expression was highest in Stem2 (**Fig 10C**), with expression per cell heterogeneous, unlike for Stem1, R, or Div cells (**Fig 10D**). A subset of Stem2 cells in NWD1 mice longer term after marking expressed higher *Ascl2* (**Fig 10D,** red arrow), a highly significant patterns by a likelihood ratio test (*P=0.01*, by a negative binomial regression-negative binomial mixed effect model, with regression and fit using R functions glm.nb and glmer.nb, respectively [53], assuming each cell as independent, and number of *Ascl2* reads for each cell as response). Post-hoc analysis by a similar negative binomial regression showed NWD1-LT differed significantly from the other 3 groups in *Ascl2* expression (*P=0.002*). Finally, potential that the difference between NWD1-LT and the other groups was random was tested using a negative binomial mixed effect model with mice per dietary group treated as random effects; the likelihood ratio test was *P = 0.11*, indicating the alternate hypothesis that effects were random is false.

In situ hybridization to fluorescent probes localized *Ascl2*^{hi} expressing cells confined to the crypt base in AIN76A mice (**Fig 10E)**, but in NWD1 mice, elevated *Ascl2* was in cells above the crypt base that co-expressed Bmi1+ (**Fig 10E**), as in mice after acute Lgr5^{hi} cell damage [17, 52], although in response to NWD1, these cells are further above the crypt (Discussion).

There are 2 early trajectory branch points among progenitor cell populations (**Fig 11A**, red arrows 1 and 2). At branch point “1”, Stem1 cells give rise to enteroendocrine, goblet and Paneth cell secretory lineages. In AIN76A mice 3d post TAM marking of Bmi1+ cells, 80% of branch point “1” cells were still Stem1, with 20% Stem2 in short term marked cells, but for NWD1 fed mice 100% of cells remained Stem1 (**Fig 11B**). Data from scRNAseq libraries of independent mice were identical. In Bmi1+ cells that had accumulated longer term after marking (66-70d post Tam), all cells at branch point “1” were Stem1 cells regardless of diet (**Fig 11C**). At branch point “2”, Stem1 cells diverged to Replicating and Dividing cells (**Fig 11A**). Shorter term

after marking, for AIN76A mice, branch 2 cells were equally distributed between R and Div cells, but longer term, shifted to 10-20% R and 80-90% Div (**Fig 11C**). However, for mice fed NWD1 either shorter or longer term, 100% of cells at branch 2 remained R cells. Dietary differences at branch point 2 were identical in replicas and highly significant for cells isolated longer and shorter term after cell marking (*P=0.001*). Bmi1+ cells in R longer term after marking express much higher *Ascl2* levels (**Fig 11D;** $P=10^{-8}$). These R cells thus express *Ascl2* at very high levels, similar to the *Bmi1+, Ascl2*^{hi} cells that accumulate above the crypt base in NWD1 mice (**Fig 10E**) and the Stem2 subset in NWD1 that express higher *Ascl2* in the Bmi1+ cells that accumulate longer term after the Bmi1+ cells and their progeny are marked (**Fig 10D**).

NWD1 reprograming of enterocytes: NWD1 altered expression profiles in all Bmi1+ cell populations both long and short term after marking, most pronounced in enterocytes, and greatest in EC7 enterocytes accumulating longer term (**Fig 12A**). EC7 is predicted to be the most mature enterocyte cell population, validated by markers that identify villus tip cells ([44], **Fig 9E)**.

The pathway most enriched in EC7 cells from Bmi1+ marked cells that accumulated longer term was antigen processing and presentation (**Fig 12B,C**; NES 1.75, *P=0.009*). CD74, a key gene in this pathway expressed in epithelial cells [54-63] that can mediate interaction between mouse Lgr5^{hi} stem cells and their immune environment [63]. The fraction of cells expressing CD74 was highly enriched across all cell clusters in the longer term marked Bmi1+ cells that accumulated with time (**Fig 12D**), paralleled by elevated expression per cell, with much higher expression in the EC7 mautre enterocytes compared to all other clusters (**Fig 12E**, $P=10^{-25}$, by negative binomial regression analysis). CD74 interacts with proteins of the major histo-compatability II (MHCII) complex to process and present cell surface antigens [58], and MHCII complex genes were also upregulated most significantly in EC7 cells (**Fig 13A**). The greatest expression of the CD74 and MHCII complex genes in EC7 cells is consistent with reported

expression of these genes predominantly in cells in the upper third of villi [64], suggesting a unique role in these differentiated cells.

Cell surface expression of CD74 characterizes dysplastic cells of the intestinal epithelium, and cells of Crohn's, Ulcerative, and Amebic colitis in the human [60, 65, 66], with chronic inflammation in each linked to elevated CRC risk. NWD1 is also pro-inflammatory, elevating serum levels of inflammatory cytokines [67], and there was a 2-3 fold increase in cells expressing CD3, a pan T cell marker, in 3 month NWD1 compared to AIN76A mice, significant when quantified as CD3 cells/villus (*P=0.008*), or percent area/villus epithelial column expressing CD3 (*P=0.015*) (**Fig 13B,C,D**).

The second most highly enriched pathway in EC7 cells in NWD1 is "Intestinal Immune Network/IgA production" (**Fig 12B,C;** NES=1.50, *P=0.027*). IgA is abundant in the intestinal and colonic mucosa, modified as it traverses the lamina propria to form an SigA complex interacting with the FcαRI receptor on myeloid cells, which is pro-inflammatory. F/480+ myeloid cells in the mucosa were also elevated by NWD1 (*P=0.01*; **Fig. 13E, F**), also characterizing pro-tumorigenic IBD [68].

The next three most highly enriched pathways in EC7 cells are *Ppar* signaling, cholesterol metabolism, and fat digestion/absorption (**Fig. 12B,C**), adaptive responses to increased fat (25%) in NWD1. In the independent scRNAseq data of the rapid dietary cross-over experiment (**Fig 7A**), fatty acid metabolism was elevated in all cell clusters by the 4-day switch to NWD1 from AIN76A, and except for Goblet2 and EE2, reverted for the clusters within 4 days of switch back to AIN76A (**Fig 12F**), consistent with rapid shift of metabolic pathways (**Fig 8A**).

A second example of an adaptive response to NWD1 was increased number of enterocytes expressing *Trpv6* in 3-month NWD1 fed mice after Bmi1+ cell marking, especially longer term (**Fig 12G**). *Trpv6* encodes the enterocyte brush border calcium channel mediating calcium uptake under low dietary calcium conditions [69]. Therefore, elevated *Trpv6* expression is the

mechanism by which NWD1 mice maintain serum calcium levels [67], despite lower calcium and vitamin D_3 in NWD1.

Dietary reprogramming by epigenetic gene modification: scATACseq libraries were generated from mice fed AIN76A or NWD1 from weaning for 4 months. Sequence analysis by Cell Ranger identified 13 clusters for the pooled libraries that were aligned with scRNAseq clusters using the Signace *"Reference Mapping"* function (NY Genome Center) (**Fig 14A**). scRNAseq had established that Stem 1 harbored canonical Lgr5^{hi} stem cells at the crypt base with trajectory analysis identifying Stem1 at initiation of maturation of all cell types/lineages (**Fig 11A**). Based on the independent scATACseq data, the number of these Stem1 cells decreased 50% in libraries from replicate NWD1 mice compared to AIN76A replicates (**Fig 14B**). Thus, the ATACseq data independently confirmed NWD1 suppression of Lgr5^{hi} cells [9, 12, 13, 70]. The position and magnitude of open chromatin regions at the promotor region of *Ppargc1a* in the Stem 1 cluster is similar for all mice (**Fig 14C**). However, in region i and ii, downstream of the promotor (expanded in **Fig 14D)**, regions of open chromatin in AIN76A mice are absent or substantially reduced in NWD1 mice, most striking for 2 areas in region ii in which peaks of open chromatin structure in *Ppargc1a* for AIN76A mice are lost in NWD1 mice. These regions in "ii" define the position of a strong enhancer with a significant role in regulating *Ppargc1a* in intestinal epithelial cells (**Fig 14D**; *Enhanceratlas 2.0*). Thus, the scATACseq data confirm NWD1 down-regulation of *Ppargc1a* expression, and establish that this is epigenetic.

The scATACseq data were interrogated for Cyp4A10, a key gene in both the NWD1 up-regulated *Ppar* and fatty acid metabolism pathways and for the NWD1 up-regulated *Trpv6* gene encoding the calcium transporter (**Fig 12F,G**). For each gene, extensive peaks of open chromatin structure were present at its promotor in NWD1 fed mice, in contrast to no detectable signal for either gene in the AIN76A control fed mice (**Fig. 15A,B**). Therefore, as for *Ppargc1a*, these two genes mediating adaptation to NWD1 were epigenetically regulated by NWD1.

Discussion:

Adjusting key nutrient exposures in the mouse to mimic those linked to elevated risk for human colon tumors causes rapid, reversible and hence dynamic adaptation of stem cells and the lineages that also alter pathogenic pathways establishing a pro-tumorigenic environment. Specific elements of this remodeling parallel the pathogenic mechanisms in human inflammatory bowel disease that is pro-tumorigenic, and the dynamic adaptation also reflects that there is dynamic plasticity in the balance of Lgr5 positive and negative stem cells that support tumor growth [26]. Thus, the mucosa at dietary risk for tumor development has already undergone complex remodeling, as documented in for both the inflamed and uninvolved mucosa in human IBD [23] and in the earliest human benign tumors [25].

NWD1 is higher in fat (25%) and lower, but not deficient, in vitamin D, calcium, methyl donors and fiber than purified control AIN76A diet on which it is based, producing a combination of key nutrient exposures for the mouse recapitulating those linked to elevated human risk for sporadic colon cancer, the vast majority of the human disease [71]. NWD1 fed mice are not obese, maintain calcium levels and bone mineral density, and reflect human metabolic syndrome: reduced energy expenditure without altered food consumption or physical activity, causing glucose intolerance, and increased pro-inflammatory cytokines [67]. NWD1 elevates Wnt signaling throughout the small and large intestinal mucosa of NWD1 [32, 72, 73], also causing ectopic expression of Paneth cell markers in cells throughout the small and large intestine [73], and recent single cell RNAseq data for the human mucosa show these markers are not restricted to Paneth cells in the human [74]. Moreover, consistent with the 50-fold increased time for intestinal stem cells of human crypts to reach crypt clonality compared to mice fed standard diets [15-17], NWD1 reduces intestinal Lgr5^{hi} cell lineage tracing, their accumulation of mutations determined by single cell whole exome sequencing, and reduces Lgr5^{hi} cell efficiency in tumor initiation, increasing these for Bmi1+ cells recruited to maintain the mucosa [9, 12, 13, 75]. The marshaling of alternate Bmi1+ cells to function as stem-like cells

parallels NWD1 expansion of the proliferative compartment above the crypt base in mice [46, 47], an expansion well-documented in humans at environmental or genetic risk for intestinal tumors [48-50].

The fact that NWD1 better reflects human risk factors for intestinal cancer, and that NWD1 fed mice uniquely develop sporadic tumors at the same incidence, frequency and developmental age as in humans [20, 22, 32] establish relevance of the diet to human risk. Although NWD1 fed mice are not a model for human IBD, there are a number of parallels between the two reinforcing this relevance and suggesting overlapping mechanisms of pathogenesis. First, in both NWD1 fed mice and human IBD, low-level chronic inflammation is pro-tumorigenic. Second, NWD1 reduced expression of *Ppargc1a* in Lgr5^{hi} cells through epigenetic alteration of the gene, mediating repression of Lgr5^{hi} cell function as stem cells in IBD [76], and single cell RNAseq has shown that human IBD is exacerbated by down regulation of the encoded protein Pgc1a [24], in both cases altering s mitochondrial structure, metabolically reprogramming the cells. Third, the most extensive reprogramming by NWD1 is in mature enterocytes at the villus tip where the most prominent NWD1 induced change is a major elevation in the interacting CD74-MHCII pathways of antigen presentation and processing. This parallels that highest expression of these pathways is in the upper villi of the human small intestine [64] and that upper crypt colonocytes exhibit greatest increase in this pathway in human IBD [23]. Moreover, NWD1 increased pro-inflammatory cytokines [67], and CD3 and myeloid cell mucosal infiltration, paralleling elevation of the CD74/MHCII pathway in human Crohn's, Ulcerative, and Amebic colitis [60, 65, 66], confirmed by single cell analysis of human IBD tissue [23], and also in H.pylori infected gastric tissue [57, 77], all chronic inflammatory states increasing risk for human tumor development. Fourth, NWD1 induces high ectopic expression of Lyz and other Paneth cell markers in mouse colon [73], similar to Lyz elevation in human IBD tissue [23] and recent single cell RNAseq data of human tissue documents expression of these markers in cells of the human mucosa that are not Paneth cells [74]. Fifth,

the extensive remodeling of stem cells and the mucosa by NWD1 demonstrate that complex remodeling characterizing the very earliest benign human tumors [25], and both the involved and uninvolved mucosa in human IBD, is already underway much earlier in the mucosa at risk. Finally, human colon tumors consist of both Lgr5 positive and negative stem cells with the balance determined by the mutational signature and environmental signals from other cell types or drugs [26], similar to what is reported here regarding the mucosa at nutritional risk that gives rise to these tumors.

The increased CD74/MHCII pathways in NWD1 fed mice, paralleling human data, contrast with a report that a 60% fat diet repressed these pathways in mouse Lgr5^{hi} cells, suggested to be pro-tumorigenic by dampening immune surveillance [78]. The different results may be due to several factors. First, there are substantial differences in dietary formulation in the two models, but with 60% dietary fat used to induce mouse obesity greatly exceeding fat intake in humans, even for obese individuals, and inducing metabolic alterations that differ from those induced by dietary fat levels more commonly encountered in the human [79, 80]. The 60% fat diet also includes the very high levels of vitamin D not seen in the human population which is a fundamental determinant of which and how stem cells function, detailed in the Introduction. Second, the repression of CD74/MHCII in the 60% dietary fat model depended on mouse microbiome composition, differing significantly among mouse rooms at the same institution [78], likely different among institutions and with different diets. Third, NWD1 elevation of the CD74/MHCII pathway is in cells derived from mobilized *Bmi1*+ cells, not a feature of the 60% fat model, with the interesting possibility that response may be a function of stem cell of origin.

The substantial remodeling of stem cells and the mucosa by NWD1 includes epigenetic regulation of pathways reflecting the rapid and reversible adaptation of the mucosa to its nutritional environment. This included NWD1 upregulated expression of *Trpv6* in enterocytes, the gut calcium transporter maintaining calcium homeostasis under low calcium conditions, explaining how, despite lower calcium in the diet, serum calcium levels are maintained with no

loss of bone mineral density [67]. A second example is the rapid and reversible alteration of pathways linked to fat metabolism in response to higher fat in NWD1. For both examples, altered expression was paralleled by substantial alteration of chromatin configuration at the gene promoter, independently confirming response to NWD1 and demonstrating epigenetic reprogramming of the cells, although post-transcriptional mechanisms across the many genes and pathways that are altered is not ruled out. These data support historic concepts of the *"milieu interiuer"* of Claude Bernard in the 1800's, and Walter Cannon's coining of the term homeostasis in the 1940's [81], each emphasizing homeostasis not as a state, but a process of continual tissue adaptation to changing environments. Thus, the now well-established plasticity of cells to de-differentiate and function as stem-like cells as a response to acute damage is expanded by the data to a normal physiological process mediating adaptation to the nutritional environment that, for the human is in constant flux.

The significance of the metabolic reprogramming of Lgr5^{hi} stem cells by NWD1 is emphasized by the necessity of Oxphos for mouse Lgr5^{hi} and Drosophila intestinal stem cells to function efficiently as stem cells [34-36], for hematopoietic stem cell functions [37], for embryonic stem cell pluripotency [38], and the role of mitochondrial function in determining whether stem cells self-renew or differentiate [45]. A consequence of the NWD1 suppression of canonical stem cell functions is recruitment of alternate *Bmi1+, Ascl2^{hi}* cells above the crypt base to maintain the mucosa, as in response to acute damage. *Ascl2* encodes a stem cell transcription factor essential for Bmi1+ cell de-differentiation in response to Lgr5^{hi} cell damage [17, 52]. *Ascl2* is regulated by Wnt signaling [82], elevated by NWD1 throughout cells of the mouse intestinal villi and the colonic mucosa [32, 72, 73]. However, the role of *Bmi1+, Ascl2^{hi}* cells may differ in dietary versus acute damage induced plasticity. Acute damage purges Lgr5^{hi} crypt base stem cells, with mobilized *Ascl2^{hi}* cells migrating into the crypt to restore crypt organization. However, limited crypt space establishes competition among crypt Lgr5^{hi} cells [17], and single cell laser ablation of crypt base cells triggers division and reorganization of remaining

stem cells, confirming importance of physical space in regulating stem cell dynamics [83]. In contrast, it is not clear whether crypt space is available with chronic NWD1 feeding. More important, Lgr5^{hi} stem cells migrating into the niche would still be repressed by NWD1, and we reported that reduced Lgr5^{hi} cell lineage tracing from the crypt base, and Oxphos and TCA pathway repression, persist to at least 1 year of feeding NWD1 [13] (and **Fig 1C,D**), and that Bmi1+ cells above the crypt base lineage trace for months in mice fed NWD1 continuously [9].

Tumors reflect successful growth advantage of transformed cells [17], but this is very rare: lower-risk individuals develop no sporadic tumors, but those at higher risk develop only 1-2 tumors despite many billions of mucosal cell divisions over decades, suggesting mechanisms establishing risk are subtle and complex. Therefore, it is fundamental that the nutritional environment, through metabolic reprogramming of stem cells, dynamically and continually sculpts the playing field on which intestinal stem cell competition takes place, with significant influence in determining outcome.

Experimental Procedures:

Mice: Mice, all on a C57Bl/6J background, were provided food and water *ad libitum* in a barrier facility at the Albert Einstein College of Medicine. For breeding, strains were fed a chow diet (Picolab 5058, Fisher Feed, Branchburg, NJ). Genotyping was by PCR of DNA from tail clips at 5 days following birth, using published primers and methods. Appropriate genotypes were randomized to purified diets (AIN76A, D10011; NWD1, D16378C; Research Diets Inc, New Brunswick, NJ). Mice of both genders were used (a total of 25 male and 20 female mice). Tamoxifen in corn oil was given as a single injection (Sigma, T5648, 100µl, 1mg/µl). Experiments were approved by the Albert Einstein Institutional Animal Care and Use Committee. All authors had access to the study data and reviewed and approved the final manuscript.

Isolation of intestinal epithelial and Lgr5^{hi} cells: *Lgr5*$^{EGFP,cre:ERT2}$ mice were sacrificed, excised intestines opened longitudinally, rinsed with cold saline, crypts isolated, single cell suspensions prepared, cells sorted by FACs, and the 2-3% of cells with highest green fluorescence collected, as described [9]

Bulk RNAseq analysis: construction of bulk RNAseq libraries, sequencing and data analysis were as described [9].

Single cell RNAseq: Intestinal cells were isolated as above, re-suspended in antibody staining buffer, blocked with FcR Blocking Reagent (Miltenyi Biotec, 05244 T-30), washed and pelleted, then incubated for 20 minutes at 4^{0}C with, EpCAM-FITC (Miltenyi Biotec, Clone caa7-9G8, Cat No. 130-123-674) and CD45-PerCP (Miltenyi Biotec, Clone 30F11, Cat No. 130-123-879). Cells were sorted by FACs on a MoFlo instrument and Epcam positive, CD45 negative total or Bmi1+ epithelial cells collected.

Single cell RNAseq (scRNAseq) libraries were constructed by the Albert Einstein Genomics Core using the 3' kit protocols of 10X Genomics (San Francisco, CA) with approximately 10,000 single FACS collected cells from each mouse loaded onto a Chromium Chip B microfluidic apparatus (10X Genomics). Library quality was verified by size analysis (BioAnalyzer; Agilent, Santa Clara, CA) and after passing quality control assays, multiple libraries were mixed and sequenced by HiSeq PE150 or NovaSeq PE150 using pair-end sequencing, with a readout length of 150 bases (Novogene; Sacramento, California), and the data assigned to individual cells using the sample indexes.

For sequence alignment and subsequent analysis, output Illumina base call files were converted to FASTQ files (bcl2fastq), these from each mouse aligned to the mouse mm10 genome v1.2.0 and converted to count matrices (Cell Ranger software v3.0.2). Force-cell parameter was used, with 5000-8000 individual cells identified for each sample, and unique molecular identifiers (UMI) identified to remove PCR duplicates. Quality control and downstream analyses were done in R v4.0.2, using Seurat package v3.2.2 [84]. To discard doublets or dead

cells, cells with gene counts <200 or >5000, or a mitochondrial gene ratio >20%, were filtered out. Cells from different samples were integrated using Seurat FindIntegrationAnchors and IntegrateData functions, clusters identified from each of integrated data set using the Seurat FindClusters function. This calculates k-nearest neighbors according to Principle Component Analysis, constructs a shared nearest neighbor graph, and then optimizes a modularity function (Louvain algorithm) to determine cell clusters. Cell clusters were identified as cell intestinal cell types using established cell-type markers and cluster identification using Seurat FindMarkers function. Differential gene expression compared samples among experimental groups: initial criteria were an expression change of ≥1.5 fold with associated adjusted P-value of <0.01 in group comparison (Seurat FindMarkers function). Pathway analysis was performed on differentially expressed genes using clusterProfiler R package v3.16.1 and the KEGG pathway database (KEGG.db R package v3.2.4); gene set enrichment analysis (GSEA) used the fgsea R package v1.14.0, the MSigDB (v5.2) hallmark gene set and the KEGG pathway database. Pathways at $P < 0.05$ were considered statistically significant. Trajectory analysis used Monocle3 R package v0.2.3.3 [85] with cluster information and cell-type identifications migrated from Seurat using an in-house computer script, the integrated dataset divided among different experimental conditions, and trajectories generated for each dietary or genetic condition.

RNAseq data have been deposited in the NCBI Gene Expression Omnibus (GEO) database: bulk RNAseq (Fig 1) - GSE186811; scRNAseq (Fig 3, *Ppargc1a* inactivation) - GSE188339; scRNAseq (Fig 4, rapid dietary crossover) - GSE188577; scRNAseq (Fig 5.6, Bmi1+ cells) - GSE188338.

***In situ* analyses:** Sections of Swiss rolls of mouse intestines fixed in 10% formalin were de-waxed and rehydrated. Reagents were from Advanced Cell Diagnostics (Newark, CA). Endogenous peroxidases were quenched and heat induced epitope retrieval done utilizing the RNAscope Multiplex Fluorescent Reagent Kit v2 (Cat. No. 323100) and the RNAscope Multiplex Fluorescent Assay v2 protocol followed. RNAscope target probes for *Bmi1* and *Ascl2*

Cat No. 466021, 412211, respectively) were hybridized to sections and amplified using the HybEZ Hybridization System (Cat No. 310010). Secondary TSA fluorophores from Akoya Biosciences were Opal 620 (channel 1, Cat No. FP1495001KT) and Opal 570 (channel 2, FP1488001KT), sections counterstained with Dapi and visualized using a Leica SP8 confocal microscope (20X magnification).

Single cell ATACseq: Total Epcam+, CD45 negative epithelial cells were isolated from the small intestine of mice by FACS as for scRNAseq analysis. Nuclei were isolated following the 10X Genomics protocol, single cell ATACseq libraries constructed using the 10X Geomics single cell ATACseq Chromium reagents and protocol, and sequenced as for the scRNAseq libraries.

Immunohistochemistry: Swiss roll sections were de-waxed, rehydrated, endogenous peroxidases blocked (3% hydrogen peroxide in methanol) and heat induced epitope retrieval done with 10 mM Sodium citrate buffer (pH 6.0) for all antibodies. Tissues were incubated overnight at 4^0C with primary CD3 antibody (Novusbio, Littleton, CO, 1:10 dilution of NB600-1441). Protein block and secondary antibody for CD3 employed ImmPRESS-Alkaline Phosphatase Horse Anti-Rabbit IgG Polymer Kit-Alkaline Phosphatase (Vector Laboratories, Burlingame, CA, Cat No. MP-5401). F4/80 antibody (1:200, Cell Signaling, Denvers, MA, Cat No. 70076, Cell Signaling, Denvers, MA) was incubated on tissue overnight at 4^0C. Secondary antibody was SignalStain® Boost IHC Detection Reagent (HRP, Rabbit, Cell Signaling, Cat No. 8114). For Pgc1a staining, tissues were incubated overnight at 4 °C overnight with rabbit anti-Pgc1a Ab (diluted 1:500, NBP1-04676, Novusbio) followed by biotinylated goat anti-rabbit IgG (1:100, BA-1000; Vector Lab,) for 30 min. The reaction was visualized using the Vectastain Elite ABC Kit (Vector Lab) and DAB Quanto kit (Thermo Fisher Scientific). Counterstaining was with hematoxylin and visualization by bright field microscopy, or a CY5 filter for CD3.

Electron Microscopy: Samples were fixed with 2.5% glutaraldehyde, 2% paraformaldehyde in 0.1 M sodium cacodylate buffer, post-fixed with 1% osmium tetroxide followed by 2% uranyl

acetate, dehydrated through a graded ethanol series and embedded in LX112 resin (LADD Research Industries, Burlington VT). Ultrathin sections were cut on a Leica Ultracut UC7, stained with uranyl acetate followed by lead citrate and viewed on a JEOL 1400 Plus transmission electron microscope at 120kv. Images were captured at a magnification of 800X, and at 5000X for quantitative measurements of mitochondrial size and cristae density.

Mitochondrial membrane potential: Crypts, isolated as reported, were dispersed into single-cell suspensions, and cells incubated with MitoTracker™ Red FM (Invitrogen, Cat # M22425, 25nM) for 20 min at 37 °C. Zombie NIR (Invitrogen, Cat # L10119) was added at the end of the incubation to mark dead cells. Flow cytometry used a Cytek Aurora Instrument (Cytek Biosciences). Data were analyzed using Flowjo 10 software (Treestar Inc.).

Lineage tracing of *Ppargc1a* knock-out mice: Induction of *cre*^{ERT2} activity was by a 100 µl intraperitoneal injection of 1 mg freshly prepared Tamoxifen (TAM) in sterile corn oil. Mice were sacrificed at 3 days after injection. Mouse intestinal tissues were fixed with 4% paraformaldehyde for 2 hrs and then hydrated with 15% sucrose for 3 hrs, and 30% sucrose for over night. Fixed tissues were embedded in optimal cutting temperature (OCT) compound (Sakura), frozen on dry ice, and sectioned by cryostat. Slides were stained with mounting solution containing DAPI for identification of nuclei before imaging.

Image analysis: To quantify anti-Pgc1a Ab staining, images were at 60x magnification. An automatically set threshold was applied for all slides and the area above threshold was calculated and divided by total area. The crypt-villus axis was divided by 20 µm increments from the base of the crypt and measured up to 80 µm. For analysis of mitochondrial morphometry, crypt base columnar cells, Paneth cells, and villus cells were imaged at 5000x magnification and selected to analyze. Cristae density was calculated by the sum of individual cristae divided by mitochondrial size. Mitochondrial size (µm^2) and cristae area (µm^2) were manually traced using Fiji. For lineage tracing quantification, the crypt-villus axis was manually traced and the threshold automatically adjusted for each crypt. Red fluorescent positive area (µm^2) was

measured and divided by total crypt-villus area (μm^2). Results were imported to GraphPad Prism version 9.4.0 for Mac, GraphPad Software, San Diego, California USA, www.graphpad.com, for visualization and statistical analysis.

Figure legends:

Figure 1: Bulk RNAseq analysis of Lgr5^{hi} cells: A, *Lgr5$^{EGFP.cre:ER}$* mice fed AIN76A or NWD1 for 3 or 12 months from weaning, or NWD1 for 3 months then switched to AIN76A for 9 months (cross-over); **B,** Expression ratio at 12 vs 3 months of 504 genes of the Lgr5^{hi} stem cell signature [10], for AIN76A or NWD1 fed mice; **C**, percent of the 504 genes with expression ratio greater or less than 1 at 12 vs 3 month for mice fed AIN76A or NWD1; **D**, number of the ~8000 expressed sequences in Lgr5^{hi} cells up or down-regulated (≥50%, *P≤0.01)* at 3 or 12 months feeding NWD1 compared to AIN76A, or 3 months NWD1 then switched to AIN76A for 9 months (Arm 3);

Figure 2: GSEA of the TCA cycle and Oxphos pathways in mice of the 3 Arms of Fig. 1A. Inserts for each panel show the NES, *P-value* and false discovery rate (FDR) for each analysis.

Figure 3: A, Expression ratio of Oxphos pathway genes in mice fed NWD1 vs AIN76A for 3 months (**Fig 1A**) or interrogation of an independent RNAseq data set from different mouse cohorts [9]; **B**, Ratio of expression in relation to diet of the 4 genes in the Oxphos pathway showing the greatest change in expression in the 2 independent data sets; **C**, summary of the down-regulated genes in relation to the subunits of each of the 5 mitochondrial electron transport chain complexes; **D,** up-regulated expression of Oxphos genes in NWD1 fed mice switched back to AIN76A at 3 months of age (Arm 3, Fig 1A).

<u>Figure 4</u>: Dietary Impact on *Ppargc1a* and mitochondria: Lgr5^{hi} cell *Ppargc1a* expression from: **A**, **B,** bulk RNAseq data bases of Fig 1A, B; **C**, interrogation of a previously reported Lgr5^{hi} cell bulk-RNA seq data bases at 3 months of feeding; **D,** immunohistochemical detection of Pgc1a in crypts of mice fed diets for 3 months; **E**, quantitation of Pgc1a immunohistochemistry in relation to position along the crypt-villus axis; **F**, *Ppargc1a* expression in Lgr5^{hi} and Bmi1+ cells from bulk RNAseq analysis of mice fed different diets for 3 months; **G**, examples of mitochondria electron microscopy images in wild-type mice fed AIN76A or NWD1, or in mice in which *Ppargc1a* was homozygously inactivated in AIN76A fed mice (800X); **H**, quantitation of mitochondrial cristae density in CBC, Paneth, and villus cells evaluated at 5000X magnification; **I,** FACs analysis of Lgr5^{hi} cell number, and **J**, Mitotracker staining of mice fed AIN76A or NWD1 for 3 months. *(*P<0.05, **0.01, ***0.001*).

<u>Figure 5</u>: Genetic inactivation of *Ppargc1a* in Lgr5 cells: A, suppressed lineage tracing from Lgr5^{hi} cells by homozygous inactivation of *Ppargc1a* in *Lgr5$^{cre:er\text{-}GFP}$, Ppargc1a$^{F/F\ or\ F/+}$, Rosa26^{tom}* mice fed control AIN76A diet, 3 days post a single Tam injection, and **B**, quantification of lineage tracing; **C,** cluster map and cell types, N=3 independent mice for each genetic group (9 scRNAseq libraries); **D**, epithelial cell distribution in clusters/lineages in wild-type mice or with heterozygous or homozygous *Ppargc1a* inactivation targeted to Lgr5^{hi} cells.

<u>Figure 6</u>: **A, B, C**, trajectory analysis of cells analyzed by scRNAseq of total intestinal epithelial cells from wild-type mice or 3 days after hetero- or homozygous *Ppargc1a* inactivation: yellow arrow, Stem cell cluster, *N=3* for each group; **D,E** cell type distribution at branch point "a" and "b" in trajectory analysis (red arrows in A, B, C) and GSEA of pathways of wild-type vs *Ppargc1a$^{-/-}$* mice at those branch points (numbers indicate *P values*); **F**, expression in the clusters of markers identified to characterize physical location of cells along the crypt villus axis

(villus bottom, mid-upper villus and villus tip) [44].

<u>Figure 7</u>: Rapid reprogramming of cells by dietary shift: A, mice fed AIN76A for 3 months (Arm1), switched to NWD1 for 4 days (Arm 2), or then switched back to AIN76A for 4 days (Arm 3); total Epcam+, CD45neg epithelial cells FACs isolated and analyzed by scRNAseq; **B**, cluster map and cell types, N=3 independent mice for each dietary Arm (9 scRNAseq libraries – Fig 7A); **C**, epithelial cell type distribution in clusters/lineages; **D**, expression in the predicted developmental trajectory of markers that identify cell position in the intestinal mucosa (villus bottom, mid-upper villi, villus tip) [44].

<u>Figure 8</u>: Effect of rapid 4 day dietary shifts on stem cells: A, B pathways significantly altered by rapid dietary shifts; minus log *P* value for significance of pathway change and magnitude of change, respectively; **C**, TCA cycle genes repressed by switching mice from AIN76A to NWD1 for 4 days and then elevated when mice were switched back to AIN76A control diet for 4 days; **D,** altered expression of each gene in the Oxphos pathway by 4 day shift from AIN76A to NWD1, and then response of each to subsequent switch back to AIN76A for 4 days.

<u>Figure 9</u>: scRNAseq of Bmi1+ intestinal epithelial cells in response to diet: A, B, Rosa26^{tom} marked Epcam+, CD45neg epithelial cells FACs isolated from *Bm1$^{cre:er}$, Rosa26^{tom}* mice fed AIN76A or NWD1 for 3 months, then sacrificed at either 3 or 66-70 days after TAM injection to activate the Rosa^{tom} marker (shorter, longer term, respectively) and cells analyzed by scRNAseq (N=2 for each group*);* **C,** cluster map of intestinal epithelial cell types/lineages**; D,** intestinal epithelial cell type/lineage distribution by diet and time post tam marking of cells: red

arrow- Stem cells**; E,** expression in the predicted developmental trajectory of markers that identify cell position in the intestinal mucosa (villus bottom, mid-upper villi, villus tip) [44].

<u>Figure 10</u>: *Ascl2* expression in Bmi1+ cells as a function of diet: A, cell trajectory analysis as a function of diet and time post marking by tamoxifen injection: Blue arrow - *Ascl2* expressing cells among stem and progenitor cells; yellow arrows, goblet and enteroendocrine cells; **B**, quantification of fraction of *Ascl2* expressing cells per cluster for each experimental group; **C**, **D,** expression of *Ascl2* per cell in Stem1, 2, Replicating and Dividing cells: red arrow in **D** denotes a Stem 2 cell population that expressed *Ascl2* at a higher level; **E,** *Ascl2* and *Bmi1* expression by *in situ* hybridization in mice fed diets for 3 months: white dotted line demarks the crypt base.

<u>Figure 11</u>: A, trajectory analysis of Bmi1+ derived cells at either 3d or 66-70 days post Tam activation of the Bmi1 marker annotated with individual cell types: red numbers/arrows denote branch points analyzed in the trajectory; **B, C** cell type distribution at branch points “1” and “2” (red arrows, trajectory analysis (Fig. 11A); **D**, *Ascl2* expression per cell at branch point 2.

<u>Figure 12</u>: NWD1 expansion of an enterocyte population: A, number of differentially expressed genes (>50% *and P=0.01*) in Bmi1 cell clusters of Fig 9C; **B,** Heat map of genes differentially expressed by diet in EC7 cells; **C,** EC7 cell pathways enriched by GSEA as a function of diet in Bmi1 cells isolated longer term post marking of Bmi1+ cells; **D**, distribution of cells expressing CD74, and **E**, CD74 expression per cell, in each cell type/lineage as a function of diet and time post marking of Bmi1+ cells; **F**, GSEA of Fatty acid metabolism pathway for all clusters by rapid dietary shift (Fig 7A); **G**, Trpv6 expression in each cell of the Bmi1+ cell

clusters in mice fed AIN76A or NWD1, shorter (top) and longer (bottom) after cell marking (Fig 9A, B).

Figure 13: An underlying inflammatory response to NWD1: A, expression of 5 genes encoding proteins of the MHCII pathway across cell type/lineages in relation to diet and shorter term (ST= 3d) or longer term (LT=66-70d) post Tam marking of Bmi1+ cells; **B**, immuno-histochemical detection of CD3+ cells in AIN76A and NWD1 fed mice; quantitation of CD3+ cells in relation to diet by number of CD3+/villus (**C**) or area of red fluorescent staining in the mucosa (**D**), N=3 mice per dietary group; **E**, F480+ cells in AIN76A and NWD1 fed mice; **F**, staining intensity per villus, N=3 mice per dietary group.

Figure 14: single cell ATAC seq data, stem cells: Wild-type mice were fed AIN76A or NWD1 for 4 months, then nuclei from total intestinal Epcam+, CD45 negative epithelial cells isolated by FACS were analyzed by single cell ATACseq. **A,** cell types and lineages identified by scATACseq; **B**, per cent Stem 1 cells in mice fed AIN76A or NWD1 based on the scATACseq data; **C,** scATACseq data for the *Ppargc1a* gene in the Stem 1 cluster; **D,** regions i and ii in C enlarged: starred brackets denote regions in which open chromatin structure in AIN76A control fed mice show no signal in NWD1 fed mice.

Figure 15: **A,** scATACseq data for the *Trpv6* gene in cells of cluster Ecx for mice fed AIN76A or NWD1; **B,** scATACseq data for the *Cyp4a10* gene in Ecx cluster for mice fed AIN76A or NWD1.

Table S1: Pathways significantly altered: GSEA of bulk RNAseq analysis of Lgr5^{hi} cells isolated by FACS from mice fed NWD1 compared to AIN76A for either 3 or 12 months, or for mice fed NWD1 for 3 months than switched back to AIN76A for 9 months, described in Fig 1A.

References cited:

[1] Keum N, Giovannucci E. Global burden of colorectal cancer: emerging trends, risk factors and prevention strategies. Nat Rev Gastroenterol Hepatol 2019;16(12):713-32.

[2] Wei EK, Colditz GA, Giovannucci EL, Wu K, Glynn RJ, Fuchs CS, Stampfer M, Willett W, Ogino S, Rosner B. A Comprehensive Model of Colorectal Cancer by Risk Factor Status and Subsite Using Data From the Nurses' Health Study. Am J Epidemiol 2017.

[3] Beyaz S, Mana MD, Roper J, Kedrin D, Saadatpour A, Hong SJ, Bauer-Rowe KE, Xifaras ME, Akkad A, Arias E, Pinello L, Katz Y, Shinagare S, Abu-Remaileh M, Mihaylova MM, Lamming DW, Dogum R, Guo G, Bell GW, Selig M, Nielsen GP, Gupta N, Ferrone CR, Deshpande V, Yuan GC, Orkin SH, Sabatini DM, Yilmaz OH. High-fat diet enhances stemness and tumorigenicity of intestinal progenitors. Nature 2016;531(7592):53-8.

[4] Beyaz S, Mana MD, Yilmaz OH. High-fat diet activates a PPAR-delta program to enhance intestinal stem cell function. Cell Stem Cell 2021;28(4):598-9.

[5] Aliluev A, Tritschler S, Sterr M, Oppenlander L, Hinterdobler J, Greisle T, Irmler M, Beckers J, Sun N, Walch A, Stemmer K, Kindt A, Krumsiek J, Tschop MH, Luecken MD, Theis FJ, Lickert H, Bottcher A. Diet-induced alteration of intestinal stem cell function underlies obesity and prediabetes in mice. Nat Metab 2021;3(9):1202-16.

[6] Simpson SJ, Le Couteur DG, Raubenheimer D. Putting the balance back in diet. Cell 2015;161(1):18-23.

[7] Warden CH, Fisler JS. Comparisons of diets used in animal models of high-fat feeding. Cell Metab 2008;7(4):277.

[8] Lien EC, Vander Heiden MG. A framework for examining how diet impacts tumour metabolism. Nat Rev Cancer 2019;19(11):651-61.

[9] Li W, Zimmerman S, Peregrina K, Houston M, Mayoral J, Zhang J, Maqbool SB, Zhang Z, Cai Y, Ye Q, Augenlicht L. The nutritional environment determines which and how intestinal stem cells contribute to homeostasis and tumorigenesis. Carcinogenesis 2019;40:937-46.

[10] Munoz J, Stange DE, Schepers AG, van de Wetering M, Koo BK, Itzkovitz S, Volckmann R, Kung KS, Koster J, Radulescu S, Myant K, Versteeg R, Sansom OJ, van Es JH, Barker N, van Oudenaarden A, Mohammed S, Heck AJ, Clevers H. The Lgr5 intestinal stem cell signature: robust expression of proposed quiescent '+4' cell markers. EMBO J 2012;31(14):3079-91.

[11] Demay MB, MacDonald PN, Skorija K, Dowd DR, Cianferotti L, Cox M. Role of the vitamin D receptor in hair follicle biology. J Steroid Biochem Mol Biol 2007;103(3-5):344-6.

[12] Li W, Peregrina K, Houston M, Augenlicht LH. Vitamin D and the nutritional environment in functions of intestinal stem cells: Implications for tumorigenesis and prevention. J Steroid Biochem Mol Biol 2019;198:105556.

[13] Peregrina K, Houston M, Daroqui C, Dhima E, Sellers RS, Augenlicht LH. Vitamin D is a determinant of mouse intestinal Lgr5 stem cell function. Carcinogenesis 2015;36:25-31.

[14] Augenlicht LH. Environmental Impact on Intestinal Stem Cell Functions in Mucosal Homeostasis and Tumorigenesis. Journal of Cellular Biochemistry 2017;118(5):943-52.

[15] Nicholson AM, Olpe C, Hoyle A, Thorsen AS, Rus T, Colombe M, Brunton-Sim R, Kemp R, Marks K, Quirke P, Malhotra S, Ten Hoopen R, Ibrahim A, Lindskog C, Myers MB, Parsons B, Tavare S, Wilkinson M, Morrissey E, Winton DJ. Fixation and Spread of Somatic Mutations in Adult Human Colonic Epithelium. Cell Stem Cell 2018;22(6):909-18 e8.

[16] Hodder MC, Flanagan DJ, Sansom OJ. Intestinal Stem Cell Dynamics: A Story of Mice and Humans. Cell Stem Cell 2018;22(6):785-7.

[17] Shivdasani RA. Race to the bottom: Darwinian competition in early intestinal tumorigenesis. Cell Stem Cell 2021;28(8):1340-2.

[18] Newmark HL. Nutrient density: an important and useful tool for laboratory animal studies. Carcinogenesis 1987;8:871-3.

[19] Newmark HL, Yang K, Kurihara N, Fan K, Augenlicht LH, Lipkin M. Western-style diet-induced colonic tumors and their modulation by calcium and vitamin D in C57Bl/6 mice: a preclinical model for human sporadic colon cancer. Carcinogenesis 2009;30(1):88-92.

[20] Newmark HL, Yang K, Lipkin M, Kopelovich L, Liu Y, Fan K, Shinozaki H. A western-style diet induces benign and malignant neoplasms in the colon of normal C57Bl//6 mice. Carcinogenesis 2001;22:1871-5.

[21] Yang K, Edelmann W, Fan K, Lau K, Leung D, Newmark H, Kucherlapati R, Lipkin M. Dietary modulation of carcinoma development in a mouse model for human familial polyposis. Cancer Res 1998;58:5713-7.

[22] Aslam MN, Paruchuri T, Bhagavathula N, Varani J. A mineral-rich red algae extract inhibits polyp formation and inflammation in the gastrointestinal tract of mice on a high-fat diet. Integr Cancer Ther 2010;9(1):93-9.

[23] Parikh K, Antanaviciute A, Fawkner-Corbett D, Jagielowicz M, Aulicino A, Lagerholm C, Davis S, Kinchen J, Chen HH, Alham NK, Ashley N, Johnson E, Hublitz P, Bao L, Lukomska J, Andev RS, Bjorklund E, Kessler BM, Fischer R, Goldin R, Koohy H, Simmons A. Colonic epithelial cell diversity in health and inflammatory bowel disease. Nature 2019;567(7746):49-55.

[24] Hou Y, Sun X, Gheinani PT, Guan X, Sharma S, Zhou Y, Jin C, Yang Z, Naren AP, Yin J, Denning TL, Gewirtz AT, Liu Y, Xie Z, Li C. Epithelial SMYD5 Exaggerates IBD by Down-regulating Mitochondrial Functions via Post-Translational Control of PGC-1alpha Stability. Cellular and molecular gastroenterology and hepatology 2022;14(2):375-403.

[25] Chen B, Scurrah CR, McKinley ET, Simmons AJ, Ramirez-Solano MA, Zhu X, Markham NO, Heiser CN, Vega PN, Rolong A, Kim H, Sheng Q, Drewes JL, Zhou Y, Southard-Smith AN, Xu Y, Ro J, Jones AL, Revetta F, Berry LD, Niitsu H, Islam M, Pelka K, Hofree M, Chen JH, Sarkizova S, Ng K, Giannakis M, Boland GM, Aguirre AJ, Anderson AC, Rozenblatt-Rosen O, Regev A, Hacohen N, Kawasaki K, Sato T, Goettel JA, Grady WM, Zheng W, Washington MK, Cai Q, Sears CL, Goldenring JR, Franklin JL, Su T, Huh WJ, Vandekar S, Roland JT, Liu Q, Coffey RJ, Shrubsole MJ, Lau KS. Differential pre-malignant programs and microenvironment chart distinct paths to malignancy in human colorectal polyps. Cell 2021;184(26):6262-80 e26.

[26] Vasquez EG, Nasreddin N, Valbuena GN, Mulholland EJ, Belnoue-Davis HL, Eggington HR, Schenck RO, Wouters VM, Wirapati P, Gilroy K, Lannagan TRM, Flanagan DJ, Najumudeen AK, Omwenga S, McCorry AMB, Easton A, Koelzer VH, East JE, Morton D, Trusolino L, Maughan T, Campbell AD, Loughrey MB, Dunne PD, Tsantoulis P, Huels DJ, Tejpar S, Sansom OJ, Leedham SJ. Dynamic and adaptive cancer stem cell population admixture in colorectal neoplasia. Cell Stem Cell 2022;29(8):1213-28 e8.

[27] Augenlicht LH, Corner G, Houston M, Laboisse C, Mariadason J, Velcich A. Microarray analysis of colonic epithelial cell maturation pathways triggered by butryate, sulindac, trichostatin A and curcumin and relationship to pathways of lineage specific differentiation. Proc Amer Assoc Cancer Res 2000.

[28] Yang WC, Mathew J, Velcich A, Edelmann W, Kucherlapati R, Lipkin M, Yang K, Augenlicht LH. Targeted inactivation of the p21 WAF1/cip1 gene enhances Apc initiated tumor formation and the tumor promoting activity of a Western-style high risk diet by altering cell maturation in the intestinal mucosa. Cancer Res 2001;61:565-9.

[29] Yang W, Bancroft,L., Nicholas, C., Lozonschi, I., Augenlicht, L.H. Targeted inactivation of p27kip1 is sufficient for large and small intestinal tumorigenesis in the mouse, which can be augmented by a western-style high-risk diet. Cancer Res 2003;63:4990-6.

[30] Yang W, Velcich A, Lozonschi I, Liang J, Nicholas C, Zhuang M, Bancroft L, Augenlicht LH. Inactivation of p21WAF1/cip1 enhances intestinal tumor formation in Muc2-/- mice. Am J Pathol 2005;166(4):1239-46.

[31] Yang K, Popova N, Yang W, Lozonschi I, Tadesse S, Kent S, Bancroft L, Matise I, Cormier R, Scherer S, Edelmann W, Lipkin M, Augenlicht L, Velcich A. Interaction of Muc2 and Apc on Wnt signaling and in intestinal tumorigenesis: potential role of chronic inflammation. Cancer Res 2008;68:7313-22.

[32] Yang K, Kurihara N, Fan K, Newmark H, Rigas B, Bancroft L, Corner G, Livote E, Lesser M, Edelmann W, Velcich A, Lipkin M, Augenlicht L. Dietary induction of colonic tumors in a mouse model of sporadic colon cancer. Cancer Res 2008;68:7803-10.

[33] Choi J, Houston M, Ye K, Wang R, Li W, Zhang X, Huffman D, Augenlicht L. Intestinal stem cell aging at single cell resolution: impairment of cell cycle and metabolic pathways and reversal by gerotherapeutics in review 2022.

[34] Rodriguez-Colman MJ, Schewe M, Meerlo M, Stigter E, Gerrits J, Pras-Raves M, Sacchetti A, Hornsveld M, Oost KC, Snippert HJ, Verhoeven-Duif N, Fodde R, Burgering BM. Interplay between metabolic identities in the intestinal crypt supports stem cell function. Nature 2017;543(7645):424-7.

[35] Chen L, Vasoya RP, Toke NH, Parthasarathy A, Luo S, Chiles E, Flores J, Gao N, Bonder EM, Su X, Verzi MP. HNF4 Regulates Fatty Acid Oxidation and Is Required for Renewal of Intestinal Stem Cells in Mice. Gastroenterology 2020;158(4):985-99 e9.

[36] Koehler CL, Perkins GA, Ellisman MH, Jones DL. Pink1 and Parkin regulate Drosophila intestinal stem cell proliferation during stress and aging. J Cell Biol 2017.

[37] Ito K, Carracedo A, Weiss D, Arai F, Ala U, Avigan DE, Schafer ZT, Evans RM, Suda T, Lee CH, Pandolfi PP. A PML-PPAR-delta pathway for fatty acid oxidation regulates hematopoietic stem cell maintenance. Nat Med 2012;18(9):1350-8.

[38] Khoa LTP, Tsan YC, Mao F, Kremer DM, Sajjakulnukit P, Zhang L, Zhou B, Tong X, Bhanu NV, Choudhary C, Garcia BA, Yin L, Smith GD, Saunders TL, Bielas SL, Lyssiotis CA, Dou Y. Histone Acetyltransferase MOF Blocks Acquisition of Quiescence in Ground-State ESCs through Activating Fatty Acid Oxidation. Cell Stem Cell 2020;27(3):441-58 e10.

[39] Bardella C, Pollard PJ, Tomlinson I. SDH mutations in cancer. Biochim Biophys Acta 2011;1807(11):1432-43.

[40] Zhang D, Wang W, Xiang B, Li N, Huang S, Zhou W, Sun Y, Wang X, Ma J, Li G, Li X, Shen S. Reduced succinate dehydrogenase B expression is associated with growth and de-differentiation of colorectal cancer cells. Tumour Biol 2013;34(4):2337-47.

[41] Wu Z, Puigserver P, Andersson U, Zhang C, Adelmant G, Mootha V, Troy A, Cinti S, Lowell B, Scarpulla RC, Spiegelman BM. Mechanisms controlling mitochondrial biogenesis and respiration through the thermogenic coactivator PGC-1. Cell 1999;98(1):115-24.

[42] Puigserver P, Spiegelman BM. Peroxisome proliferator-activated receptor-gamma coactivator 1 alpha (PGC-1 alpha): transcriptional coactivator and metabolic regulator. Endocr Rev 2003;24(1):78-90.

[43] D'Errico I, Salvatore L, Murzilli S, Lo Sasso G, Latorre D, Martelli N, Egorova AV, Polishuck R, Madeyski-Bengtson K, Lelliott C, Vidal-Puig AJ, Seibel P, Villani G, Moschetta A. Peroxisome proliferator-activated receptor-gamma coactivator 1-alpha (PGC1alpha) is a metabolic regulator of intestinal epithelial cell fate. Proc Natl Acad Sci U S A 2011;108(16):6603-8.

[44] Moor AE, Harnik Y, Ben-Moshe S, Massasa EE, Rozenberg M, Eilam R, Bahar Halpern K, Itzkovitz S. Spatial Reconstruction of Single Enterocytes Uncovers Broad Zonation along the Intestinal Villus Axis. Cell 2018;175(4):1156-67 e15.

[45] Iwata R, Casimir P, Vanderhaeghen P. Mitochondrial dynamics in postmitotic cells regulate neurogenesis. Science 2020;369(6505):858-62.

[46] Newmark HL, Lipkin M, Maheshwari N. Colonic hyperplasia and hyperproliferation induced by a nutritional stress diet with four components of westen-style diet. J Nat Cancer Inst 1990;82:491-6.

[47] Newmark HL, Lipkin M, Maheshwari N. Colonic hyperproliferation induced in rats and mice by nutritional-stress diets containing four components of a human western-style diet (series 2). Am J Clin Nutr 1991;54:209S-14S.

[48] Lipkin M, Winawer SJ, Sherlock P. Early identification of individuals at increased risk for cancer of the large intestine. Part I: Definition of high risk populations. Clin Bull 1981;11:13-21.

[49] Lipkin M, Blattner WE, Fraumeni JF, Lynch HT, Deschner E, Winawer S. Tritiated thymidine (0p,0h)labeling distribution as a marker for hereditary predisposition to colon cancer. Cancer Res 1983;43:1899-904.

[50] Lipkin M, Newmark H. Effect of added dietary calcium on colonic epithelial cell proliferation in subjects at high-risk for familial colon cancer. NEnglJMed 1985;313:1381-4.

[51] Lipkin M, Friedman E, Winawer SJ, Newmark H. Colonic epithelial cell proliferation in responders and nonresponders to supplemental dietary calcium. Cancer Res 1989;49:248-54.

[52] Murata K, Jadhav U, Madha S, van Es J, Dean J, Cavazza A, Wucherpfennig K, Michor F, Clevers H, Shivdasani RA. Ascl2-Dependent Cell Dedifferentiation Drives Regeneration of Ablated Intestinal Stem Cells. Cell Stem Cell 2020;26(3):377-90 e6.

[53] Bates D, Mächler M, B B, Walker S. Fitting Linear Mixed-Effects Models Using lme4. Journal of Statistical Software 2015;67(1):1-48.

[54] Volc-Platzer B, Majdic O, Knapp W, Wolff K, Hinterberger W, Lechner K, Stingl G. Evidence of HLA-DR antigen biosynthesis by human keratinocytes in disease. J Exp Med 1984;159(6):1784-9.

[55] Collins T, Korman AJ, Wake CT, Boss JM, Kappes DJ, Fiers W, Ault KA, Gimbrone MA, Jr., Strominger JL, Pober JS. Immune interferon activates multiple class II major histocompatibility complex genes and the associated invariant chain gene in human endothelial cells and dermal fibroblasts. Proc Natl Acad Sci U S A 1984;81(15):4917-21.

[56] Momburg F, Koch N, Moller P, Moldenhauer G, Butcher GW, Hammerling GJ. Differential expression of Ia and Ia-associated invariant chain in mouse tissues after in vivo treatment with IFN-gamma. J Immunol 1986;136(3):940-8.

[57] Beswick EJ, Reyes VE. CD74 in antigen presentation, inflammation, and cancers of the gastrointestinal tract. World J Gastroenterol 2009;15(23):2855-61.

[58] Schroder B. The multifaceted roles of the invariant chain CD74--More than just a chaperone. Biochim Biophys Acta 2016;1863(6 Pt A):1269-81.

[59] Jiang Z, Xu M, Savas L, LeClair P, Banner BF. Invariant chain expression in colon neoplasms. Virchows Arch 1999;435(1):32-6.

[60] Ishigami S, Natsugoe S, Tokuda K, Nakajo A, Iwashige H, Aridome K, Hokita S, Aikou T. Invariant chain expression in gastric cancer. Cancer Lett 2001;168(1):87-91.

[61] Gold DV, Stein R, Burton J, Goldenberg DM. Enhanced expression of CD74 in gastrointestinal cancers and benign tissues. Int J Clin Exp Pathol 2010;4(1):1-12.

[62] Tamori Y, Tan X, Nakagawa K, Takai E, Akagi J, Kageshita T, Egami H, Ogawa M. Clinical significance of MHC class II-associated invariant chain expression in human gastric carcinoma. Oncol Rep 2005;14(4):873-7.

[63] Biton M, Haber AL, Rogel N, Burgin G, Beyaz S, Schnell A, Ashenberg O, Su CW, Smillie C, Shekhar K, Chen Z, Wu C, Ordovas-Montanes J, Alvarez D, Herbst RH, Zhang M, Tirosh I, Dionne D, Nguyen LT, Xifaras ME, Shalek AK, von Andrian UH, Graham DB, Rozenblatt-Rosen O, Shi HN, Kuchroo V, Yilmaz OH, Regev A, Xavier RJ. T Helper Cell Cytokines Modulate Intestinal Stem Cell Renewal and Differentiation. Cell 2018;175(5):1307-20 e22.

[64] Wosen JE, Mukhopadhyay D, Macaubas C, Mellins ED. Epithelial MHC Class II Expression and Its Role in Antigen Presentation in the Gastrointestinal and Respiratory Tracts. Front Immunol 2018;9:2144.

[65] de Jong YP, Abadia-Molina AC, Satoskar AR, Clarke K, Rietdijk ST, Faubion WA, Mizoguchi E, Metz CN, Alsahli M, ten Hove T, Keates AC, Lubetsky JB, Farrell RJ, Michetti P, van Deventer SJ, Lolis E, David JR, Bhan AK, Terhorst C. Development of chronic colitis is dependent on the cytokine MIF. Nat Immunol 2001;2(11):1061-6.

[66] Lawrance IC, Fiocchi C, Chakravarti S. Ulcerative colitis and Crohn's disease: distinctive gene expression profiles and novel susceptibility candidate genes. Hum Mol Genet 2001;10(5):445-56.

[67] Bastie C, Gaffney-Stomberg E, Ting-Wen L, Dhima E, Pessin J, Augenlicht L. Dietary cholecalcifero and calcium levels in a western-style defined rodent diet alter energy metabolism and inflammatory response in mice. J Nutrition 2012;142:859-65.

[68] Breedveld A, van Egmond M. IgA and FcalphaRI: Pathological Roles and Therapeutic Opportunities. Front Immunol 2019;10:553.

[69] Suzuki Y, Landowski CP, Hediger MA. Mechanisms and regulation of epithelial Ca2+ absorption in health and disease. Annu Rev Physiol 2008;70:257-71.

[70] Augenlicht LH. Environmental Impact on Intestinal Stem Cell Functions in Mucosal Homeostasis and Tumorigenesis. J Cell Biochem 2017;118(5):943-52.

[71] Newmark HL, Yang K, Lipkin M, Kopelovich L, Liu Y, Fan K, Shinozaki H. A Western-style diet induces benign and malignant neoplasms in the colon of normal C57Bl/6 mice. Carcinogenesis 2001;22(11):1871-5.

[72] Augenlicht LH, Taylor J, Anderson L, Lipkin M. Patterns of gene expression that characterize the colonic mucosa in patients at genetic risk for colonic cancer. ProcNatlAcadSciUSA 1991;88:3286-9.

[73] Wang D, Peregrina K, Dhima E, Lin EY, Mariadason JM, Augenlicht LH. Paneth cell marker expression in intestinal villi and colon crypts characterizes dietary induced risk for mouse sporadic intestinal cancer. Proc Natl Acad Sci U S A 2011;108(25):10272-7.

[74] Burclaff J, Bliton RJ, Breau KA, Ok MT, Gomez-Martinez I, Ranek JS, Bhatt AP, Purvis JE, Woosley JT, Magness ST. A Proximal-to-Distal Survey of Healthy Adult Human Small Intestine and Colon Epithelium by Single-Cell Transcriptomics. Cellular and molecular gastroenterology and hepatology 2022;13(5):1554-89.

[75] Augenlicht L. Environmental Impact on Intestinal Stem Cell Functions in Mucosal Homeostasis and Tumorigenesis. Journal of Cellular Biochemistry 2017;118:943-52.

[76] Davidson LA, Goldsby JS, Callaway ES, Shah MS, Barker N, Chapkin RS. Alteration of colonic stem cell gene signatures during the regenerative response to injury. Biochim Biophys Acta 2012;1822(10):1600-7.

[77] Xia HH, Lam SK, Chan AO, Lin MC, Kung HF, Ogura K, Berg DE, Wong BC. Macrophage migration inhibitory factor stimulated by Helicobacter pylori increases proliferation of gastric epithelial cells. World J Gastroenterol 2005;11(13):1946-50.

[78] Beyaz S, Chung C, Mou H, Bauer-Rowe KE, Xifaras ME, Ergin I, Dohnalova L, Biton M, Shekhar K, Eskiocak O, Papciak K, Ozler K, Almeqdadi M, Yueh B, Fein M, Annamalai D, Valle-Encinas E, Erdemir A, Dogum K, Shah V, Alici-Garipcan A, Meyer HV, Ozata DM, Elinav E, Kucukural A, Kumar P, McAleer JP, Fox JG, Thaiss CA, Regev A, Roper J, Orkin SH, Yilmaz OH. Dietary suppression of MHC class II expression in intestinal epithelial cells enhances intestinal tumorigenesis. Cell Stem Cell 2021;28(11):1922-35 e5.

[79] Speakman JR. Use of high-fat diets to study rodent obesity as a model of human obesity. Int J Obes (Lond) 2019;43(8):1491-2.

[80] Bastias-Perez M, Serra D, Herrero L. Dietary Options for Rodents in the Study of Obesity. Nutrients 2020;12(11).

[81] Davies KJ. Adaptive homeostasis. Molecular aspects of medicine 2016;49:1-7.

[82] Schuijers J, Junker JP, Mokry M, Hatzis P, Koo BK, Sasselli V, van der Flier LG, Cuppen E, van Oudenaarden A, Clevers H. Ascl2 acts as an R-spondin/Wnt-responsive switch to control stemness in intestinal crypts. Cell Stem Cell 2015;16(2):158-70.

[83] Choi J, Rakhilin N, Gadamsetty P, Joe DJ, Tabrizian T, Lipkin SM, Huffman DM, Shen X, Nishimura N. Intestinal crypts recover rapidly from focal damage with coordinated motion of stem cells that is impaired by aging. Scientific reports 2018;8(1):10989.

[84] Stuart T, Butler A, Hoffman P, Hafemeister C, Papalexi E, Mauck WM, 3rd, Hao Y, Stoeckius M, Smibert P, Satija R. Comprehensive Integration of Single-Cell Data. Cell 2019;177(7):1888-902 e21.

[85] Trapnell C, Cacchiarelli D, Grimsby J, Pokharel P, Li S, Morse M, Lennon NJ, Livak KJ, Mikkelsen TS, Rinn JL. The dynamics and regulators of cell fate decisions are revealed by pseudotemporal ordering of single cells. Nat Biotechnol 2014;32(4):381-6.

1008

Figures, Choi et al, CMGH

Fig. 1

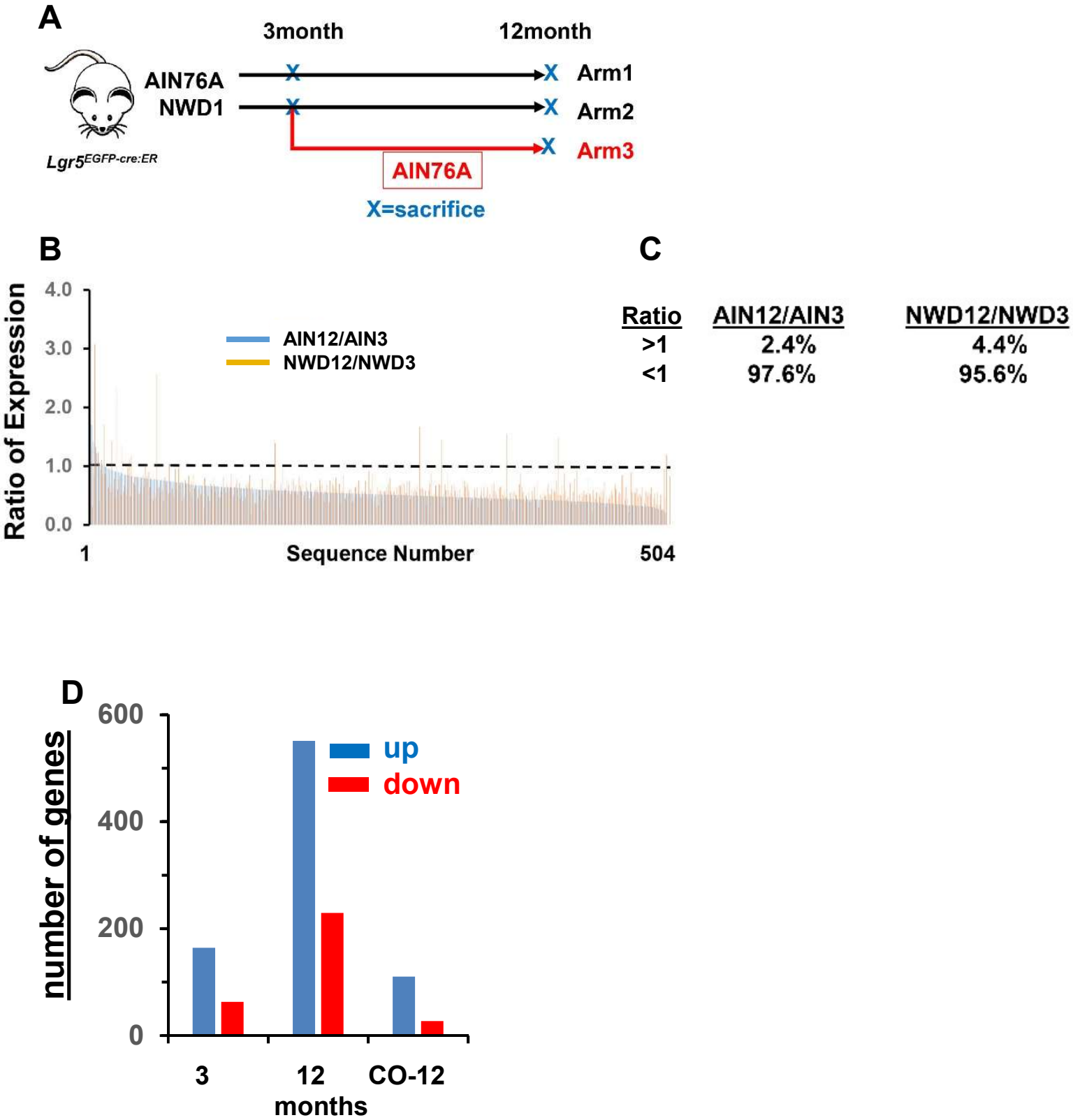

Figure 1: Bulk RNAseq analysis of Lgr5^{hi} cells: A, *Lgr5$^{EGFP.cre:ER}$* mice fed AIN76A or NWD1 for 3 or 12 months from weaning, or NWD1 for 3 months then switched to AIN76A for 9 months (cross-over); **B,** Expression ratio at 12 vs 3 months of 504 genes of the Lgr5^{hi} stem cell signature [10], for AIN76A or NWD1 fed mice; **C**, percent of the 504 genes with expression ratio greater or less than 1 at 12 vs 3 month for mice fed AIN76A or NWD1; **D**, number of the ~8000 expressed sequences in Lgr5^{hi} cells up or down-regulated (≥50%, *P≤0.01)* at 3 or 12 months feeding NWD1 compared to AIN76A, or 3 months NWD1 then switched to AIN76A for 9 months (Arm 3);

Fig. 2

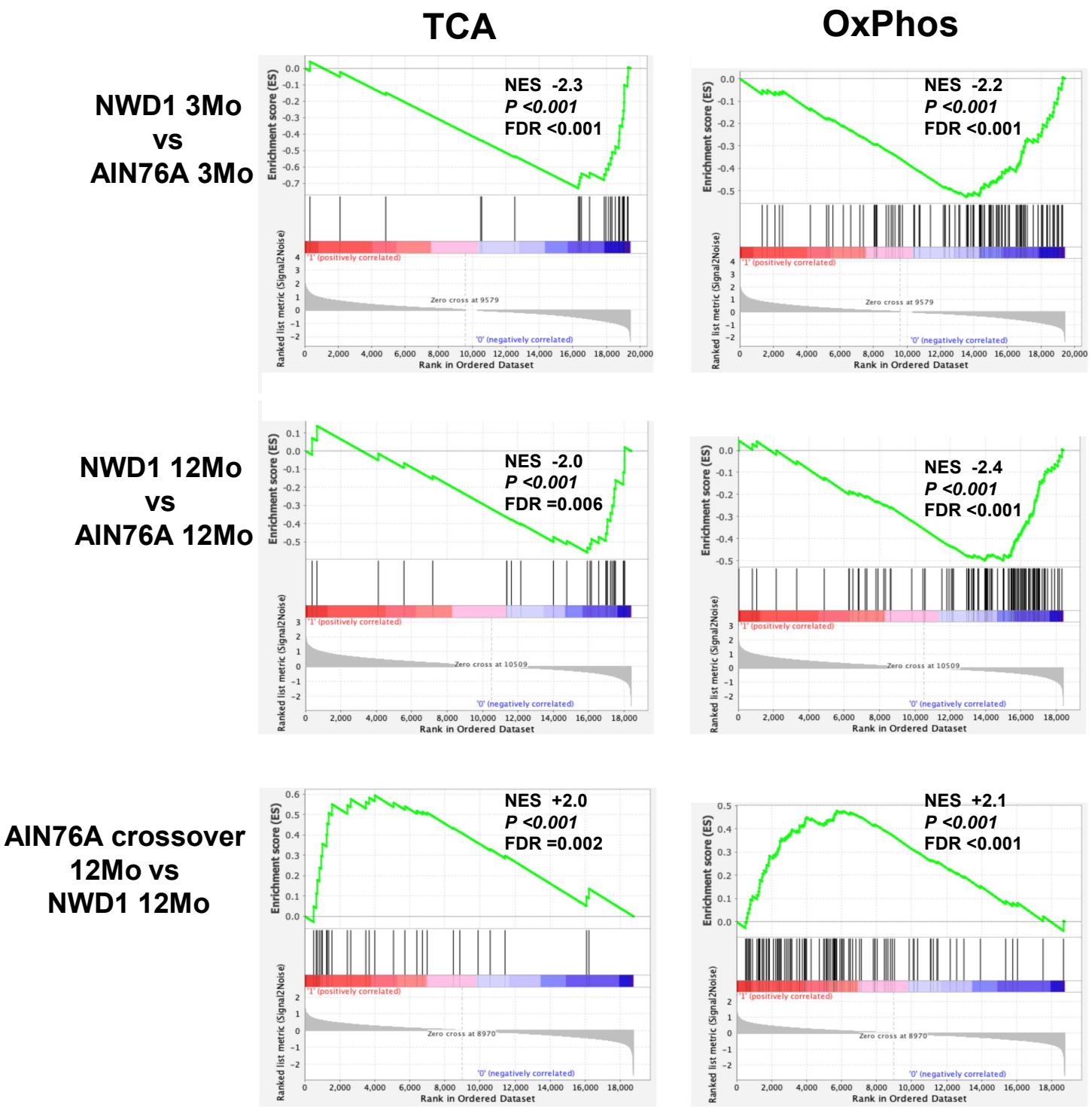

Figure 2: GSEA of the TCA cycle and Oxphos pathways in mice of the 3 Arms of Fig. 1A. Inserts for each panel show the NES, *P-value* and false discovery rate (FDR) for each analysis.

Fig. 3

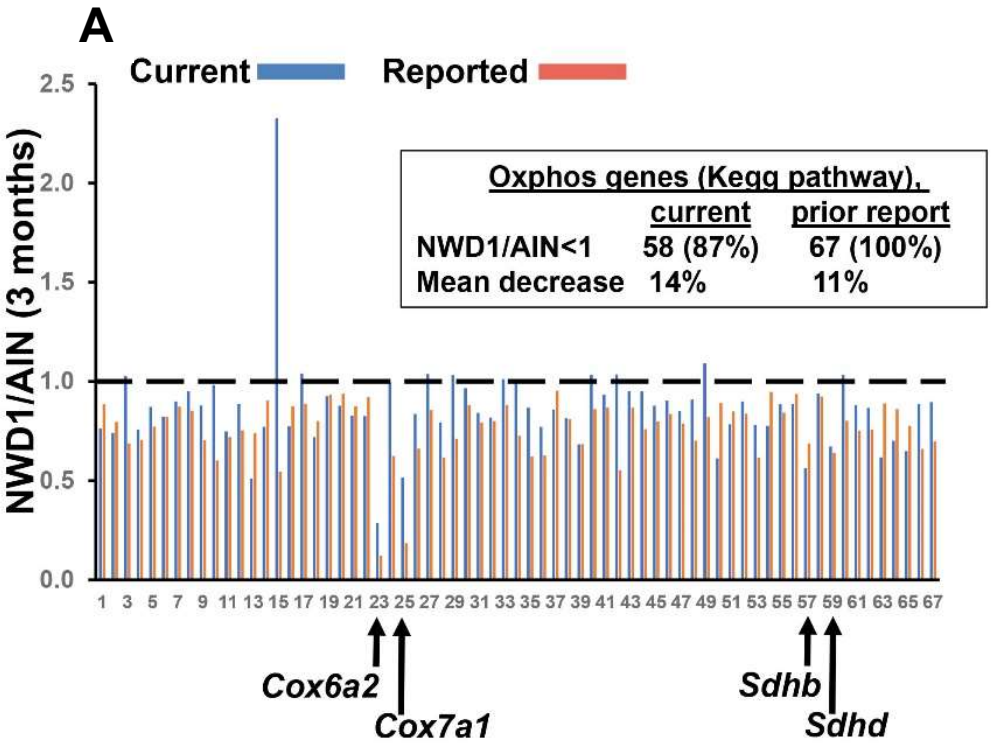

B

	NWD1/AIN76A	
	Current	Reported
Cox6a2	0.29	0.12
Cox7a1	0.52	0.19
Sdhb	0.56	0.69
Sdhd	0.67	0.64

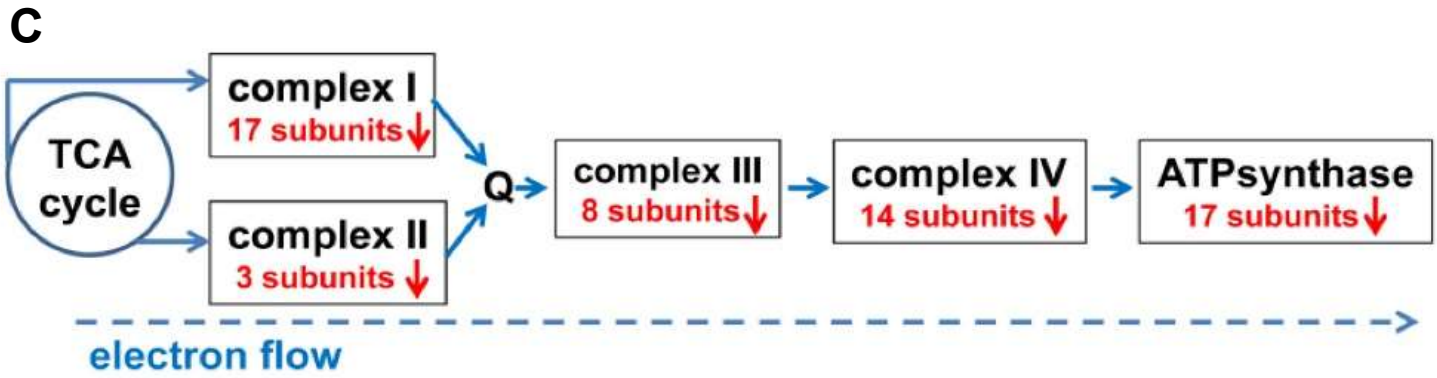

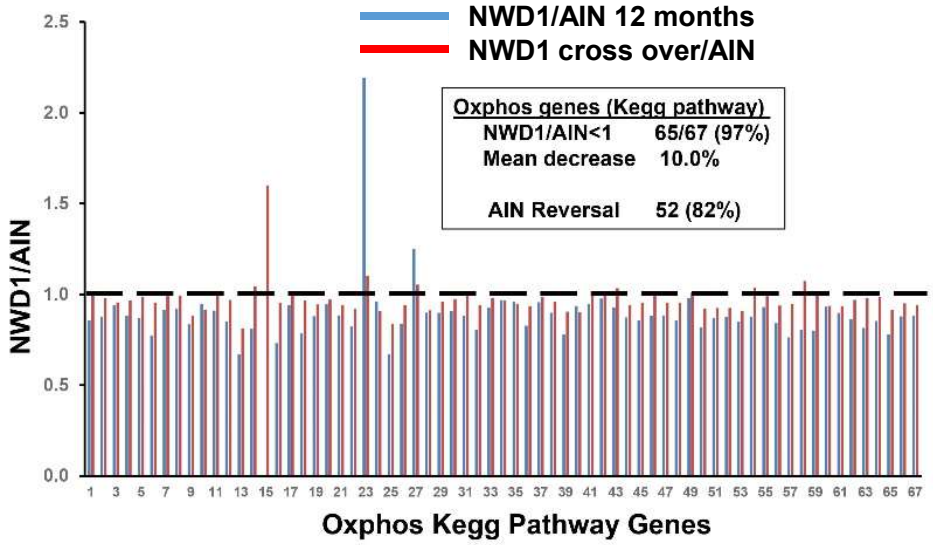

<u>Figure 3</u>: A, Expression ratio of Oxphos pathway genes in mice fed NWD1 vs AIN76A for 3 months (**Fig 1A**) or interrogation of an independent RNAseq data set from different mouse cohorts [9]; **B**, Ratio of expression in relation to diet of the 4 genes in the Oxphos pathway showing the greatest change in expression in the 2 independent data sets; **C**, summary of the down-regulated genes in relation to the subunits of each of the 5 mitochondrial electron transport chain complexes; **D,** up-regulated expression of Oxphos genes in NWD1 fed mice switched back to AIN76A at 3 months of age (Arm 3, Fig 1A).

Fig. 4

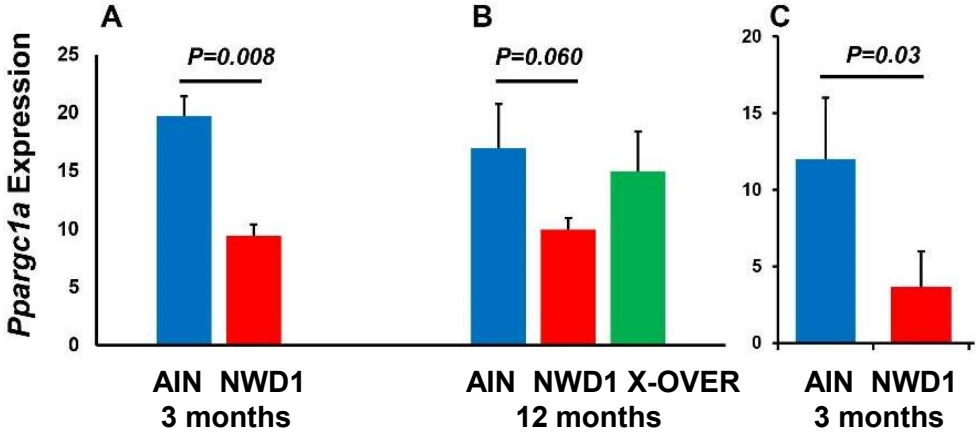
A
B
C
Ppargc1a Expression
P=0.008
P=0.060
P=0.03
AIN NWD1
3 months
AIN NWD1 X-OVER
12 months
AIN NWD1
3 months

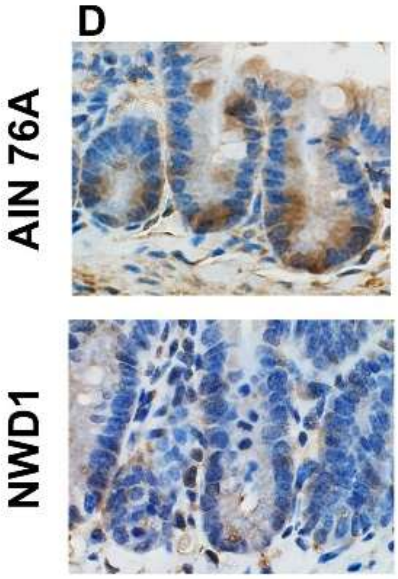
D
AIN 76A
NWD1

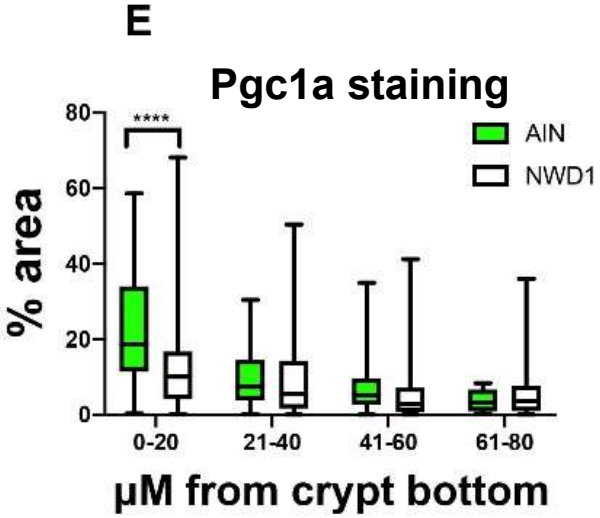
E
Pgc1a staining
AIN
NWD1
% area
****
0-20
21-40
41-60
61-80
µM from crypt bottom

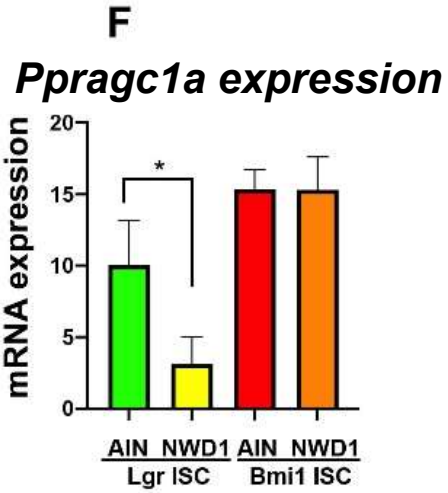
F
Ppragc1a expression
mRNA expression
*
AIN NWD1
Lgr ISC
AIN NWD1
Bmi1 ISC

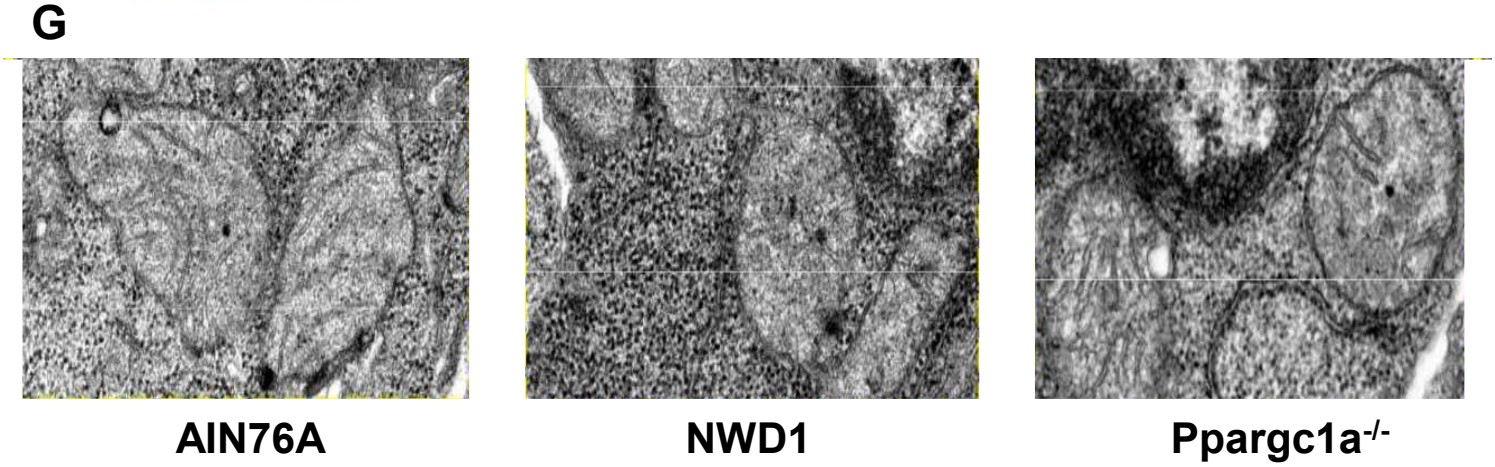
G
AIN76A
NWD1
Ppargc1a-/-

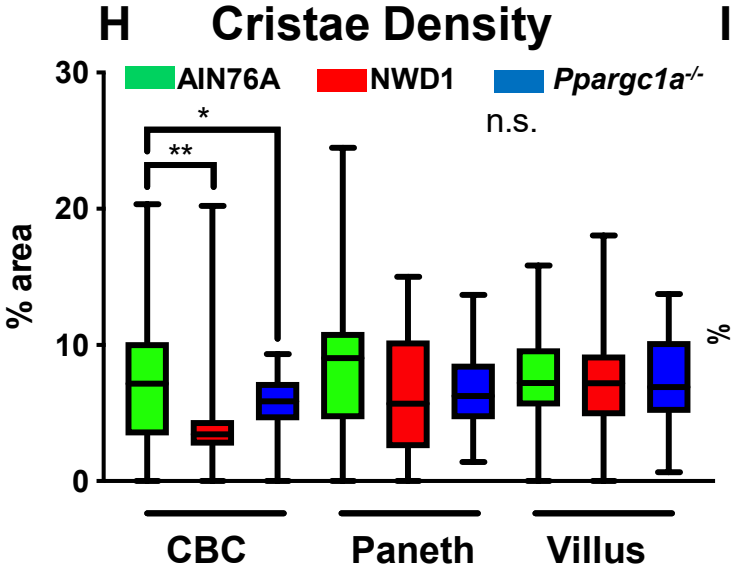
H Cristae Density
AIN76A
NWD1
Ppargc1a-/-
% area
*
**
n.s.
CBC
Paneth
Villus

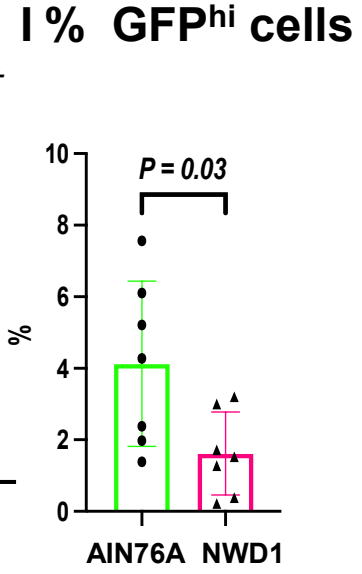
I % GFPhi cells
P = 0.03
%
AIN76A
NWD1

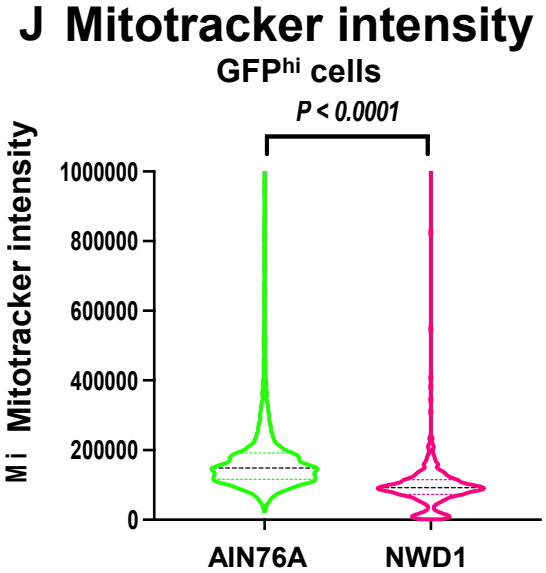
J Mitotracker intensity
GFPhi cells
P < 0.0001
Mi Mitotracker intensity
AIN76A
NWD1

<u>Figure 4</u>: Dietary Impact on *Ppargc1a* and mitochondria: Lgr5^{hi} cell *Ppargc1a* expression from: **A**, **B,** bulk RNAseq data bases of Fig 1A, B; **C**, interrogation of a previously reported Lgr5^{hi} cell bulk-RNA seq data bases at 3 months of feeding; **D,** immunohistochemical detection of Pgc1a in crypts of mice fed diets for 3 months; **E**, quantitation of Pgc1a immunohistochemistry in relation to position along the crypt-villus axis; **F**, *Ppargc1a* expression in Lgr5^{hi} and Bmi1+ cells from bulk RNAseq analysis of mice fed different diets for 3 months; **G**, examples of mitochondria electron microscopy images in wild-type mice fed AIN76A or NWD1, or in mice in which *Ppargc1a* was homozygously inactivated in AIN76A fed mice (800X); **H**, quantitation of mitochondrial cristae density in CBC, Paneth, and villus cells evaluated at 5000X magnification; **I,** FACs analysis of Lgr5^{hi} cell number, and **J**, Mitotracker staining of mice fed AIN76A or NWD1 for 3 months. *(*P<0.05, **0.01, ***0.001*).

Fig. 5

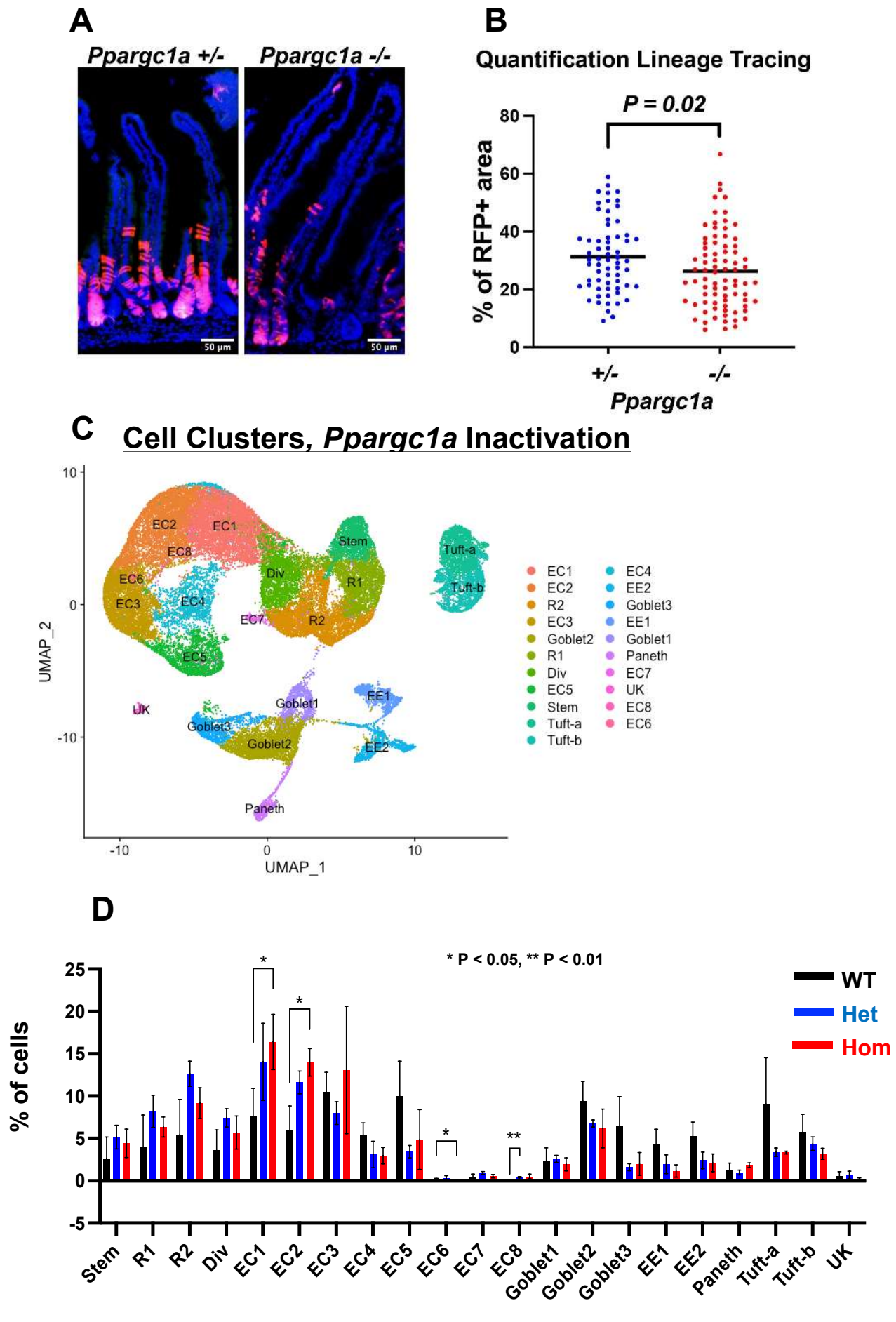
A
Ppargc1a +/-
Ppargc1a -/-
50 µm
50 µm
B
Quantification Lineage Tracing
P = 0.02
% of RFP+ area
80
60
40
20
0
+/-
-/-
Ppargc1a
C
Cell Clusters, Ppargc1a Inactivation
UMAP_2
UMAP_1
10
0
-10
-10
0
10
EC2
EC1
EC8
EC6
EC3
EC4
EC7
EC5
Div
Stem
R1
R2
Tuft-a
Tuft-b
UK
Goblet1
Goblet3
Goblet2
EE1
EE2
Paneth
EC1
EC2
R2
EC3
Goblet2
R1
Div
EC5
Stem
Tuft-a
Tuft-b
EC4
EE2
Goblet3
EE1
Goblet1
Paneth
EC7
UK
EC8
EC6
D
* P < 0.05, ** P < 0.01
WT
Het
Hom
% of cells
25
20
15
10
5
0
-5
*
*
*
**
Stem
R1
R2
Div
EC1
EC2
EC3
EC4
EC5
EC6
EC7
EC8
Goblet1
Goblet2
Goblet3
EE1
EE2
Paneth
Tuft-a
Tuft-b
UK

<u>Figure 5</u>: Genetic inactivation of *Ppargc1a* in Lgr5 cells: A, suppressed lineage tracing from Lgr5^{hi} cells by homozygous inactivation of *Ppargc1a* in *Lgr5$^{cre:er\text{-}GFP}$, Ppargc1a$^{F/F\ or\ F/+}$, Rosa26^{tom}* mice fed control AIN76A diet, 5 days post a single Tam injection, and **B**, quantification of lineage tracing; **C,** cluster map and cell types, N=3 independent mice for each genetic group (9 scRNAseq libraries); **D**, epithelial cell distribution in clusters/lineages in wild-type mice or with heterozygous or homozygous *Ppargc1a* inactivation targeted to Lgr5^{hi} cells.

Fig 6

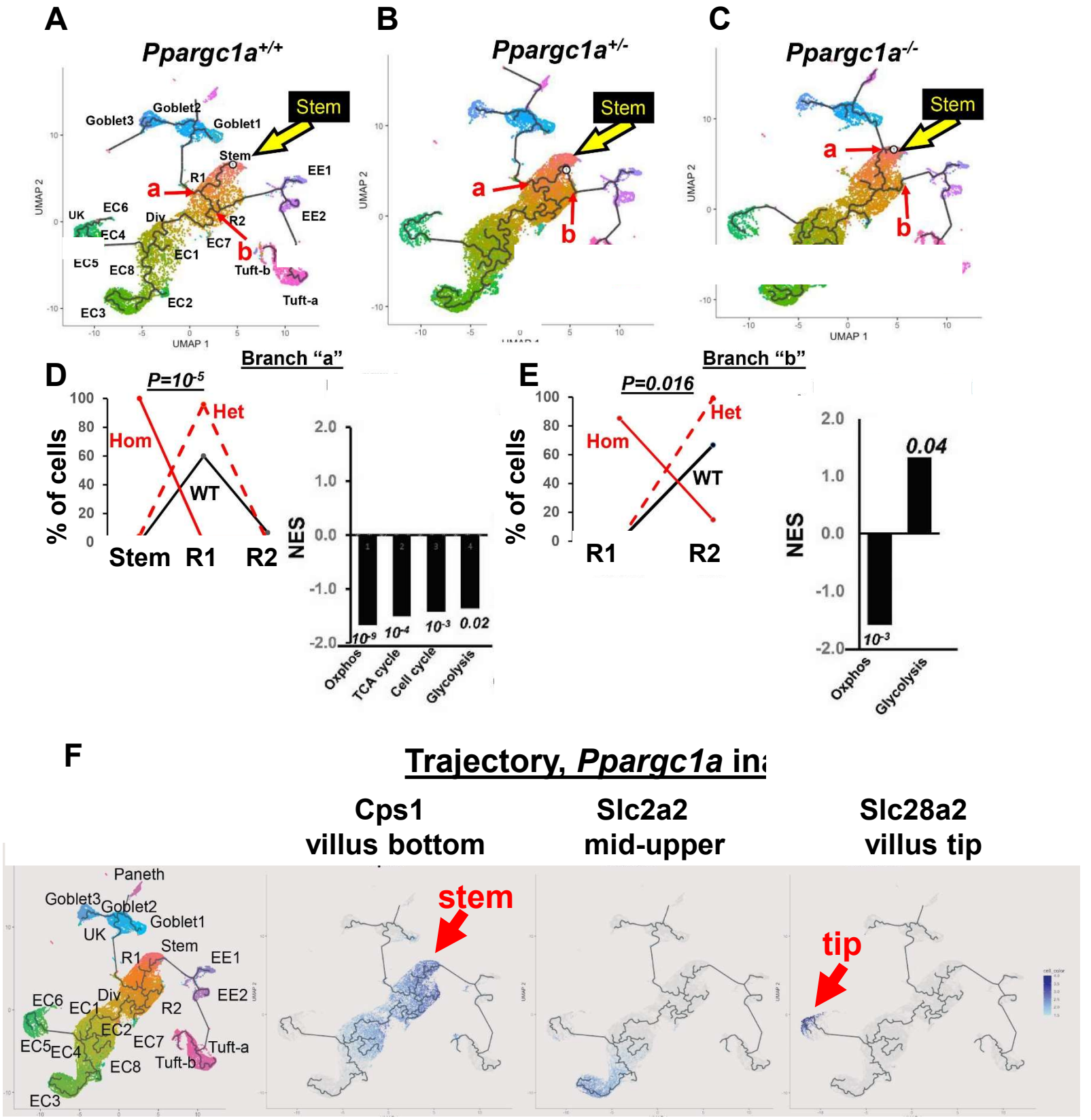

Figure 6: **A, B, C**, trajectory analysis of cells analyzed by scRNAseq of total intestinal epithelial cells from wild-type mice or 3 days after hetero- or homozygous *Ppargc1a* inactivation: yellow arrow, Stem cell cluster, *N=3* for each group; **D,E** cell type distribution at branch point "a" and "b" in trajectory analysis (red arrows in A, B, C) and GSEA of pathways of wild-type vs *Ppargc1a*$^{-/-}$ mice at those branch points (numbers indicate *P values*); **F**, expression in the clusters of markers identified to characterize physical location of cells along the crypt villus axis (villus bottom, mid-upper villus and villus tip) [44].

Fig. 7

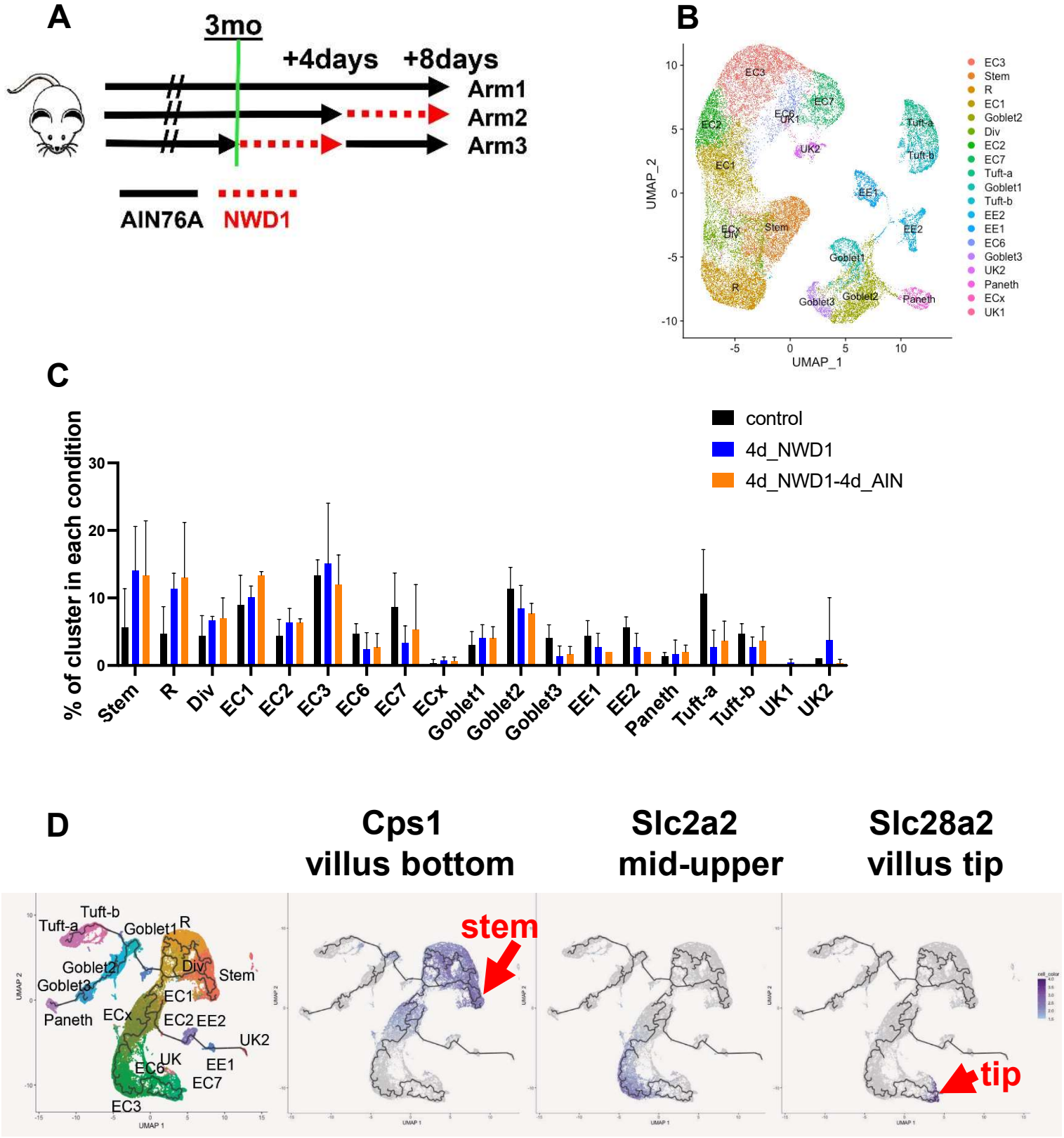

Figure 7: Rapid reprogramming of cells by dietary shift: A, mice fed AIN76A for 3 months (Arm1), switched to NWD1 for 4 days (Arm 2), or then switched back to AIN76A for 4 days (Arm 3); total Epcam+, CD45neg epithelial cells FACs isolated and analyzed by scRNAseq; **B**, cluster map and cell types, N=3 independent mice for each dietary Arm (9 scRNAseq libraries – Fig 7A); **C**, epithelial cell type distribution in clusters/lineages; **D**, expression in the predicted developmental trajectory of markers that identify cell position in the intestinal mucosa (villus bottom, mid-upper villi, villus tip) [44].

Fig. 8

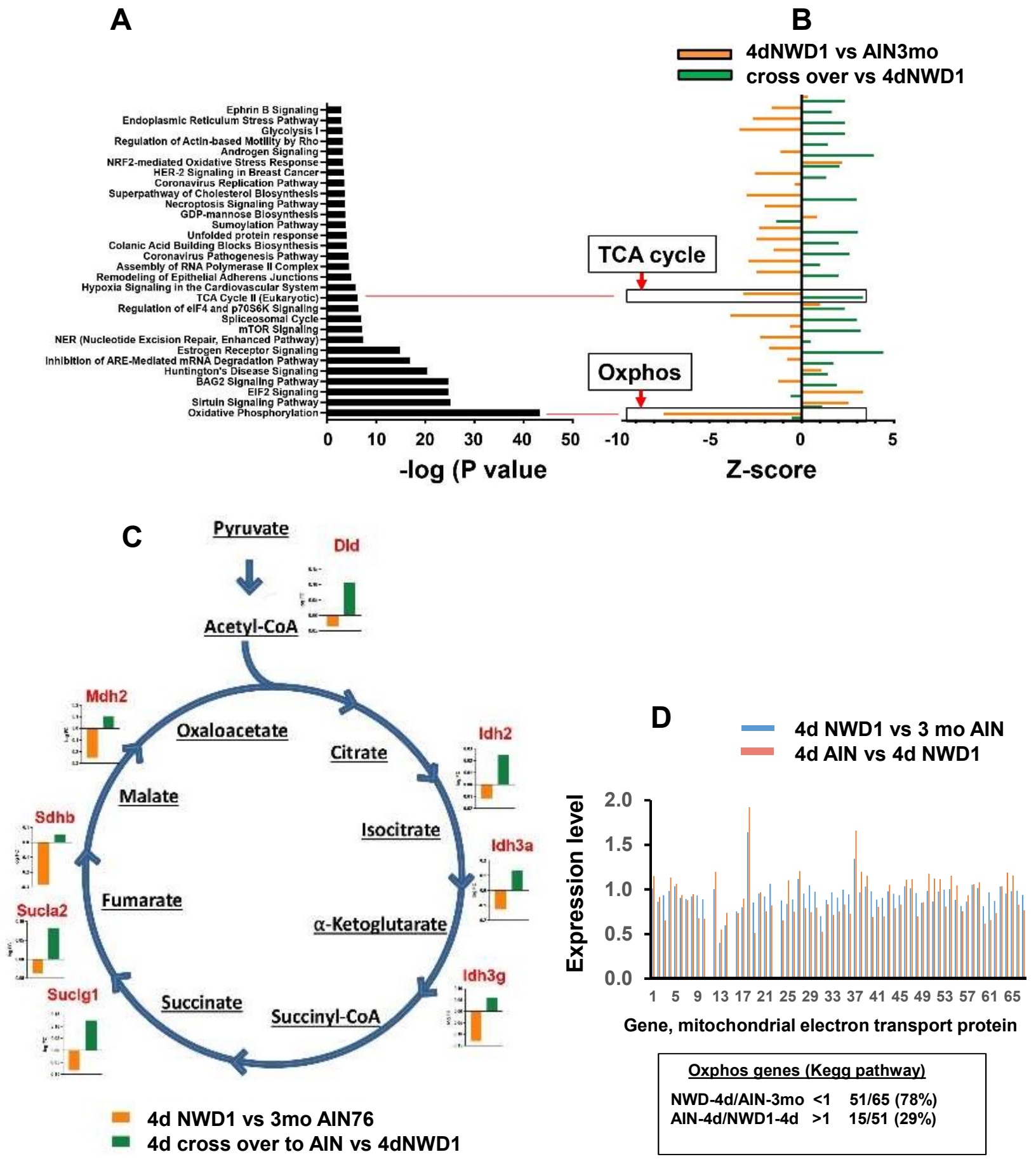
A
B
4dNWD1 vs AIN3mo
cross over vs 4dNWD1
Ephrin B Signaling
Endoplasmic Reticulum Stress Pathway
Glycolysis I
Regulation of Actin-based Motility by Rho
Androgen Signaling
NRF2-mediated Oxidative Stress Response
HER-2 Signaling in Breast Cancer
Coronavirus Replication Pathway
Superpathway of Cholesterol Biosynthesis
Necroptosis Signaling Pathway
GDP-mannose Biosynthesis
Sumoylation Pathway
Unfolded protein response
Colanic Acid Building Blocks Biosynthesis
Coronavirus Pathogenesis Pathway
Assembly of RNA Polymerase II Complex
Remodeling of Epithelial Adherens Junctions
Hypoxia Signaling in the Cardiovascular System
TCA Cycle II (Eukaryotic)
Regulation of eIF4 and p70S6K Signaling
Spliceosomal Cycle
mTOR Signaling
NER (Nucleotide Excision Repair, Enhanced Pathway)
Estrogen Receptor Signaling
Inhibition of ARE-Mediated mRNA Degradation Pathway
Huntington's Disease Signaling
BAG2 Signaling Pathway
EIF2 Signaling
Sirtuin Signaling Pathway
Oxidative Phosphorylation
TCA cycle
Oxphos
0 10 20 30 40 50
-log (P value
-10 -5 0 5
Z-score
C
Pyruvate
Dld
Acetyl-CoA
Mdh2
Oxaloacetate
Citrate
Idh2
Malate
Isocitrate
Sdhb
Idh3a
Fumarate
Sucla2
α-Ketoglutarate
Idh3g
Suclg1
Succinate
Succinyl-CoA
4d NWD1 vs 3mo AIN76
4d cross over to AIN vs 4dNWD1
D
4d NWD1 vs 3 mo AIN
4d AIN vs 4d NWD1
Expression level
2.0
1.5
1.0
0.5
0.0
1 5 9 13 17 21 25 29 33 37 41 45 49 53 57 61 65
Gene, mitochondrial electron transport protein
Oxphos genes (Kegg pathway)
NWD-4d/AIN-3mo <1 51/65 (78%)
AIN-4d/NWD1-4d >1 15/51 (29%)

<u>Figure 8</u>: Effect of rapid 4 day dietary shifts on stem cells: A, B pathways significantly altered by rapid dietary shifts; minus log *P* value for significance of pathway change and magnitude of change, respectively; **C**, TCA cycle genes repressed by switching mice from AIN76A to NWD1 for 4 days and then elevated when mice were switched back to AIN76A control diet for 4 days; **D,** altered expression of each gene in the Oxphos pathway by 4 day shift from AIN76A to NWD1, and then response of each to subsequent switch back to AIN76A for 4 days.

Fig 9

A

Cell Clusters, *Bmi1 Cells*

B

scRNAseq libraries

diet (3mo)	days post-TAM	
NWD1	3	shorter term
NWD1	3	
AIN76A	3	
AIN76A	3	
NWD1	66	longer term
NWD1	70	
AIN76A	66	
AIN76A	70	

C

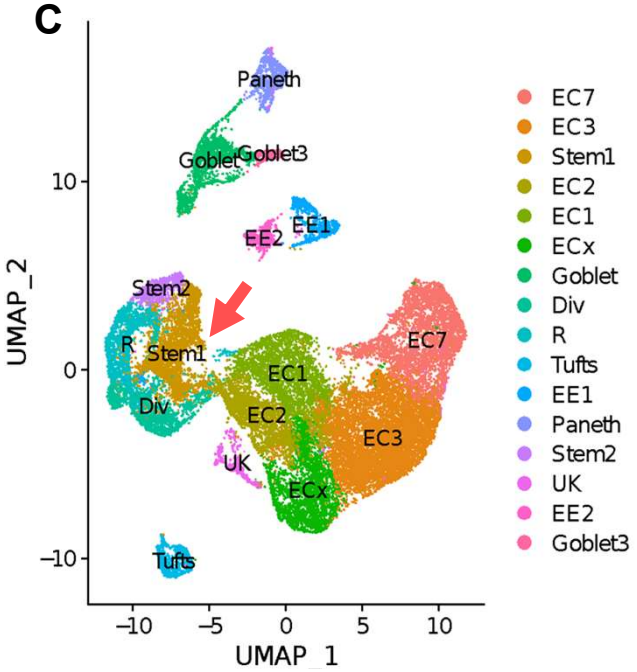

D

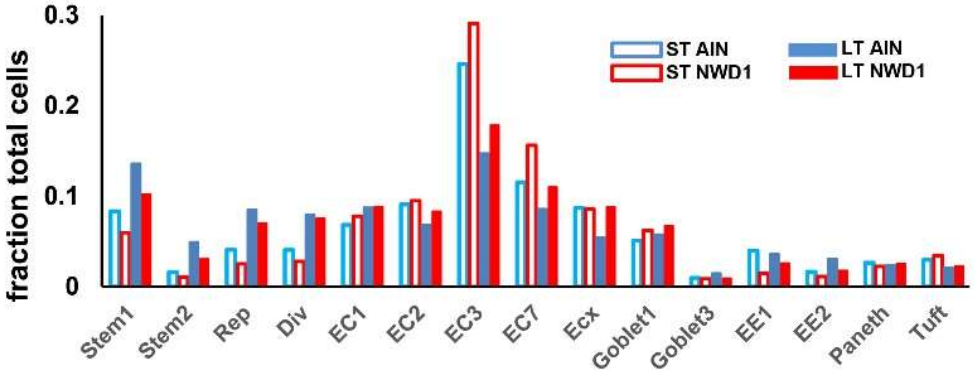

Trajectory, Bmi1+ cells

E

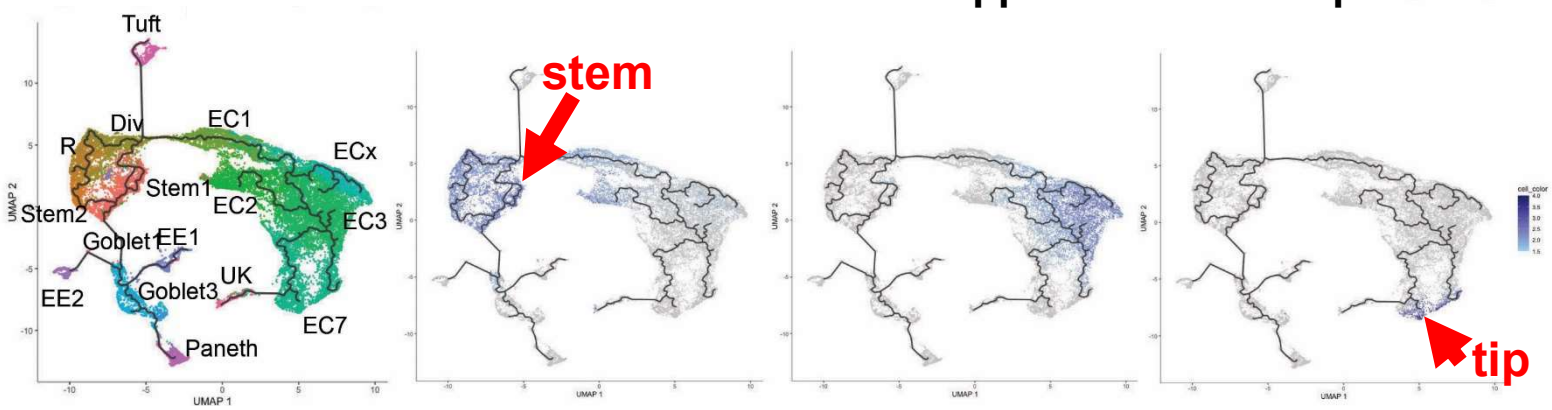

<u>Figure 9</u>: scRNAseq of Bmi1+ intestinal epithelial cells in response to diet: A, B, Rosa26^{tom} marked Epcam+, CD45neg epithelial cells FACs isolated from *Bm1$^{cre:er}$, Rosa26^{tom}* mice fed AIN76A or NWD1 for 3 months, then sacrificed at either 3 or 66-70 days after TAM injection to activate the Rosa^{tom} marker (shorter, longer term, respectively) and cells analyzed by scRNAseq (N=2 for each group*);* **C,** cluster map of intestinal epithelial cell types/lineages**; D,** intestinal epithelial cell type/lineage distribution by diet and time post tam marking of cells: red arrow- Stem cells**; E,** expression in the predicted developmental trajectory of markers that identify cell position in the intestinal mucosa (villus bottom, mid-upper villi, villus tip) [44].

Fig.10

A

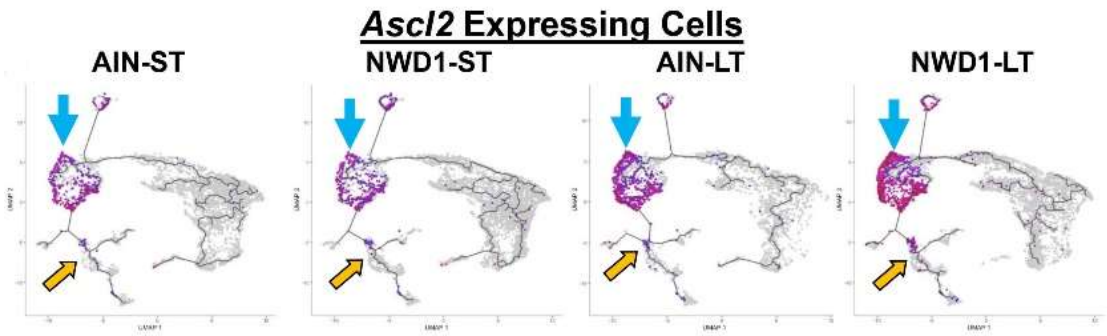
Ascl2 Expressing Cells
AIN-ST
NWD1-ST
AIN-LT
NWD1-LT

B

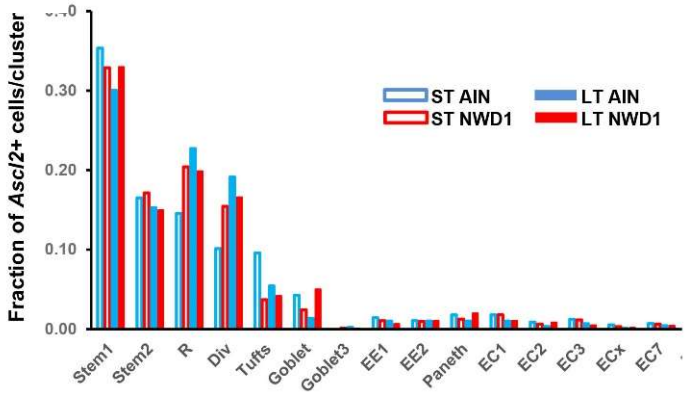
Fraction of Ascl2+ cells/cluster
0.30
0.20
0.10
0.00
ST AIN
ST NWD1
LT AIN
LT NWD1
Stem1
Stem2
R
Div
Tufts
Goblet
Goblet3
EE1
EE2
Paneth
EC1
EC2
EC3
ECx
EC7

C

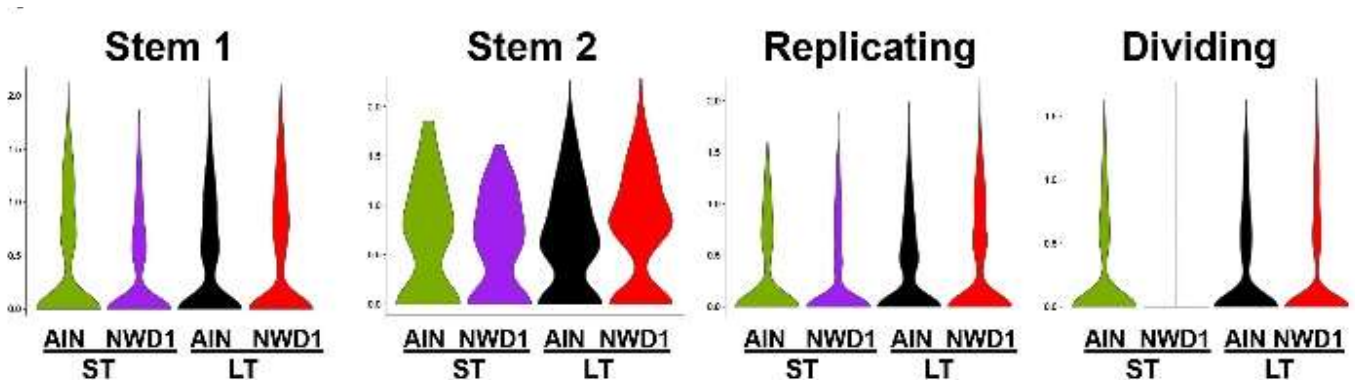
Stem 1
Stem 2
Replicating
Dividing
AIN NWD1
ST
AIN NWD1
LT

D

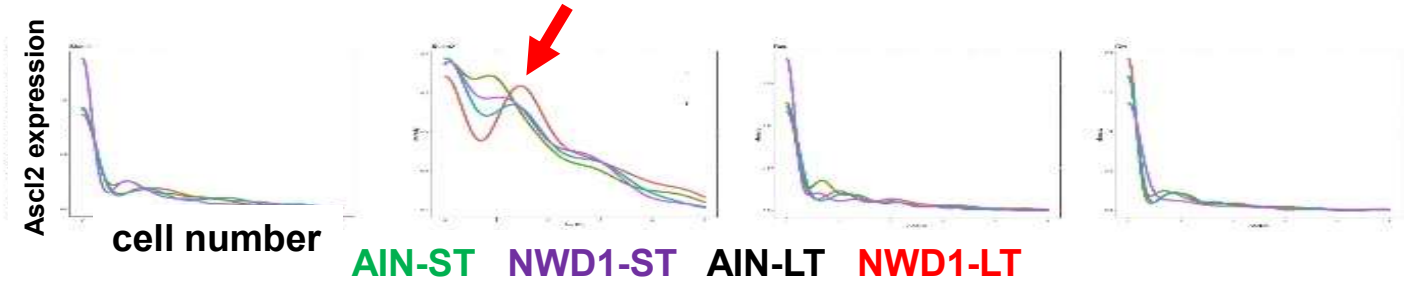
Ascl2 expression
cell number
AIN-ST
NWD1-ST
AIN-LT
NWD1-LT

E

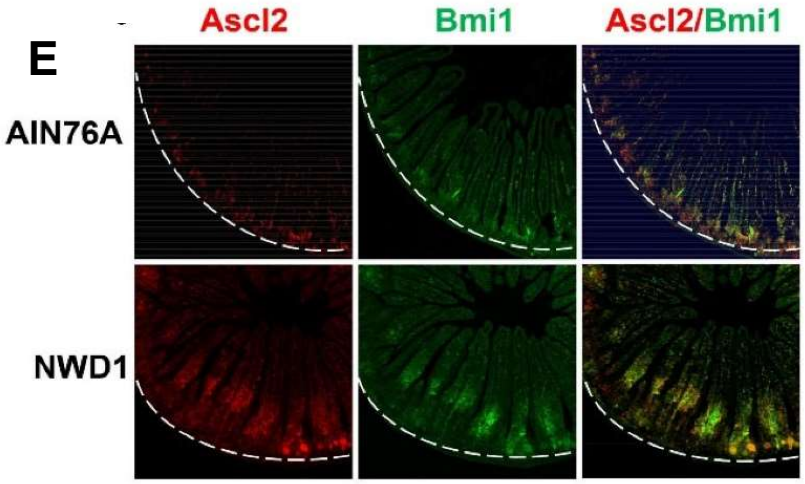
Ascl2
Bmi1
Ascl2/Bmi1
AIN76A
NWD1

<u>Figure 10</u>: *Ascl2* expression in Bmi1+ cells as a function of diet: A, cell trajectory analysis as a function of diet and time post marking by tamoxifen injection: Blue arrow - *Ascl2* expressing cells among stem and progenitor cells; yellow arrows, goblet and enteroendocrine cells; **B**, quantification of fraction of *Ascl2* expressing cells per cluster for each experimental group; **C**, **D,** expression of *Ascl2* per cell in Stem1, 2, Replicating and Dividing cells: red arrow in **D** denotes a Stem 2 cell population that expressed *Ascl2* at a higher level; **E,** *Ascl2* and *Bmi1* expression by *in situ* hybridization in mice fed diets for 3 months: white dotted line demarks the crypt base.

Fig 11

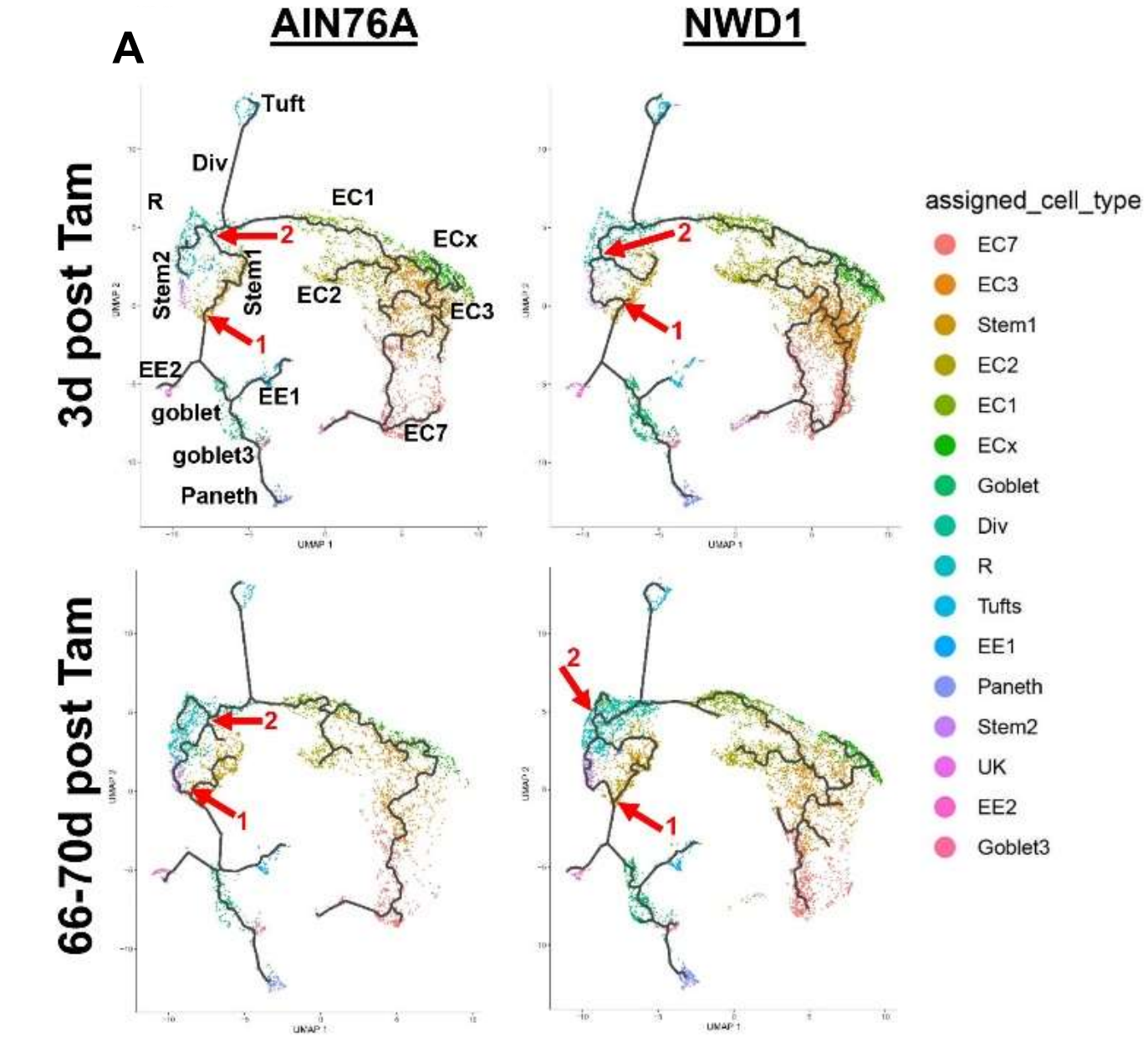
A
AIN76A
NWD1
3d post Tam
66-70d post Tam
Tuft
Div
R
EC1
ECx
Stem2
Stem1
EC2
EC3
EE2
EE1
goblet
EC7
goblet3
Paneth
1
2
UMAP 1
UMAP 2
assigned_cell_type
EC7
EC3
Stem1
EC2
EC1
ECx
Goblet
Div
R
Tufts
EE1
Paneth
Stem2
UK
EE2
Goblet3

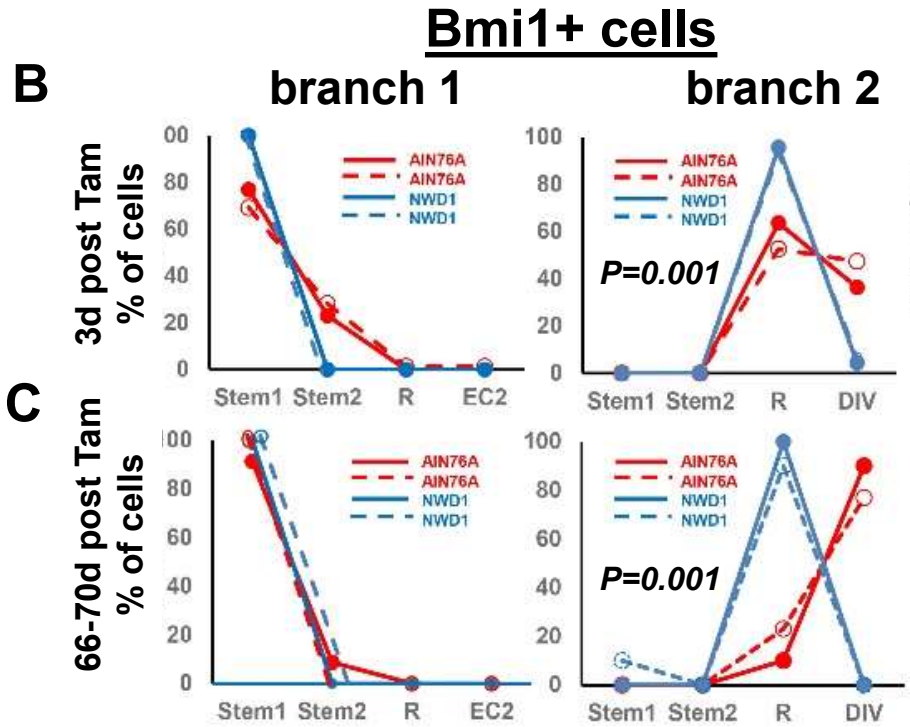
Bmi1+ cells
B
branch 1
branch 2
3d post Tam
% of cells
C
66-70d post Tam
% of cells
AIN76A
AIN76A
NWD1
NWD1
P=0.001
P=0.001
Stem1
Stem2
R
EC2
DIV
0
20
40
60
80
100

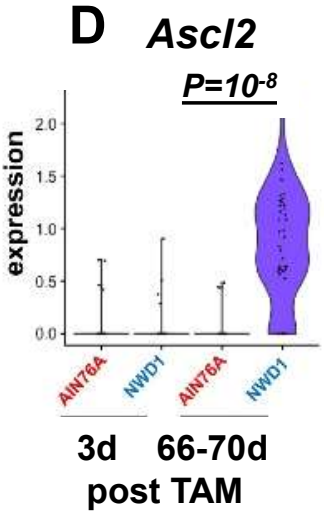
D
Ascl2
P=10-8
expression
0.0
0.5
1.0
1.5
2.0
AIN76A
NWD1
AIN76A
NWD1
3d
66-70d
post TAM

<u>Figure 11</u>: A, trajectory analysis of Bmi1+ derived cells at either 3d or 66-70 days post Tam activation of the Bmi1 marker annotated with individual cell types: red numbers/arrows denote branch points analyzed in the trajectory; **B, C** cell type distribution at branch points “1” and “2” (red arrows, trajectory analysis (Fig. 11A); **D**, *Ascl2* expression per cell at branch point 2.

Fig. 12

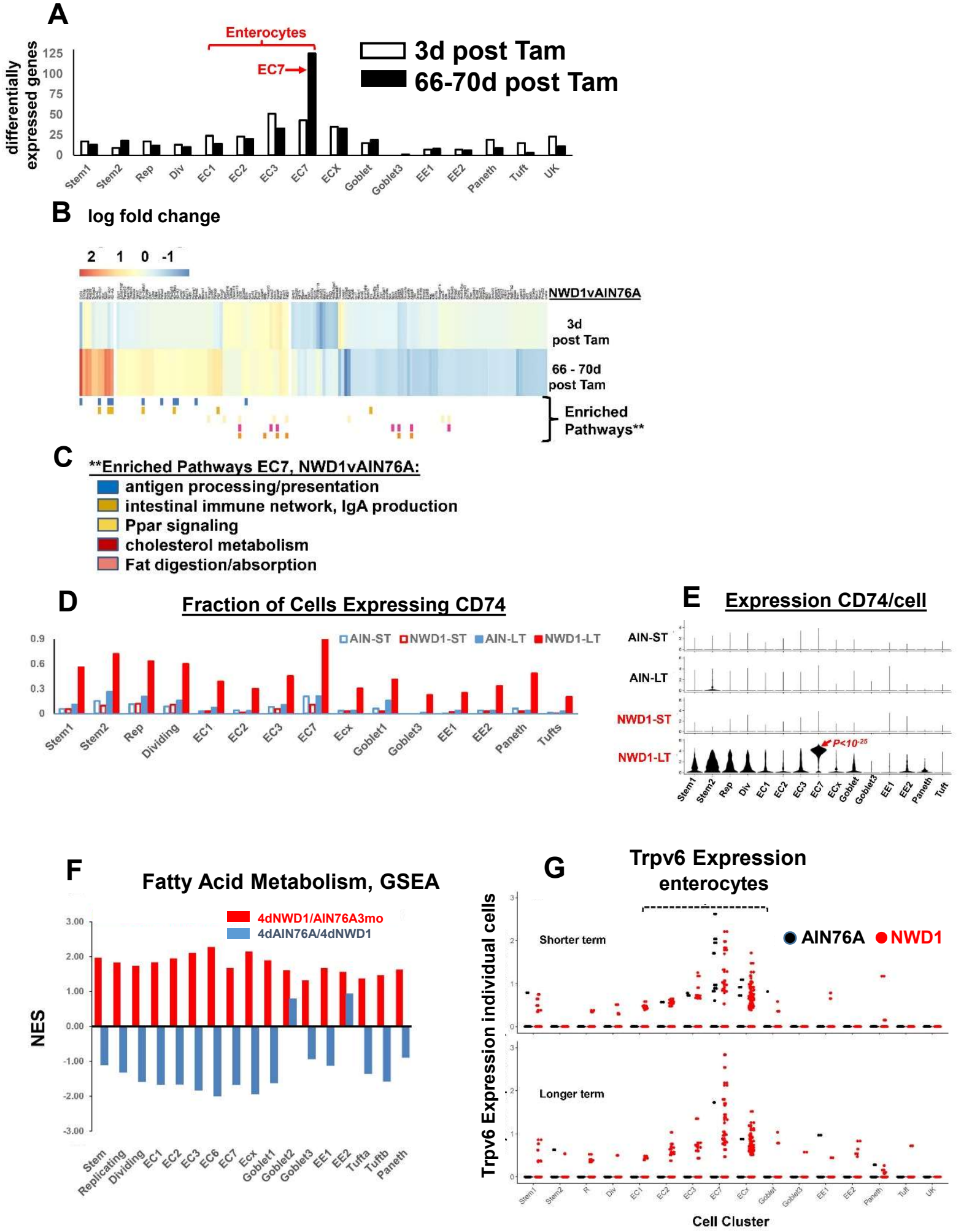
A
Enterocytes
EC7
3d post Tam
66-70d post Tam
differentially expressed genes
125
100
75
50
25
0
Stem1
Stem2
Rep
Div
EC1
EC2
EC3
EC7
ECX
Goblet
Goblet3
EE1
EE2
Paneth
Tuft
UK
B
log fold change
2
1
0
-1
NWD1vAIN76A
3d post Tam
66 - 70d post Tam
Enriched Pathways**
C
**Enriched Pathways EC7, NWD1vAIN76A:
antigen processing/presentation
intestinal immune network, IgA production
Ppar signaling
cholesterol metabolism
Fat digestion/absorption
D
Fraction of Cells Expressing CD74
AIN-ST
NWD1-ST
AIN-LT
NWD1-LT
0.9
0.6
0.3
0
Stem1
Stem2
Rep
Dividing
EC1
EC2
EC3
EC7
Ecx
Goblet1
Goblet3
EE1
EE2
Paneth
Tufts
E
Expression CD74/cell
AIN-ST
AIN-LT
NWD1-ST
NWD1-LT
P<10-25
Stem1
Stem2
Rep
Div
EC1
EC2
EC3
EC7
ECx
Goblet
Goblet3
EE1
EE2
Paneth
Tuft
F
Fatty Acid Metabolism, GSEA
4dNWD1/AIN76A3mo
4dAIN76A/4dNWD1
NES
3.00
2.00
1.00
0.00
-1.00
-2.00
-3.00
Stem
Replicating
Dividing
EC1
EC2
EC3
EC6
EC7
Ecx
Goblet1
Goblet2
Goblet3
EE1
EE2
Tufta
Tuftb
Paneth
G
Trpv6 Expression
enterocytes
Shorter term
Longer term
AIN76A
NWD1
Trpv6 Expression individual cells
Cell Cluster
Stem1
Stem2
R
Div
EC1
EC2
EC3
EC7
ECx
Goblet
Goblet3
EE1
EE2
Paneth
Tuft
UK

<u>Figure 12</u>: NWD1 expansion of an enterocyte population: A, number of differentially expressed genes (>50% *and P=0.01*) in Bmi1 cell clusters of Fig 9C; **B,** Heat map of genes differentially expressed by diet in EC7 cells; **C,** EC7 cell pathways enriched by GSEA as a function of diet in Bmi1 cells isolated longer term post marking of Bmi1+ cells; **D**, distribution of cells expressing CD74, and **E**, CD74 expression per cell, in each cell type/lineage as a function of diet and time post marking of Bmi1+ cells; **F**, GSEA of Fatty acid metabolism pathway for all clusters by rapid dietary shift (Fig 7A); **G**, Trpv6 expression in each cell of the Bmi1+ cell clusters in mice fed AIN76A or NWD1, shorter (top) and longer (bottom) after cell marking (Fig 9A, B).

Fig 13

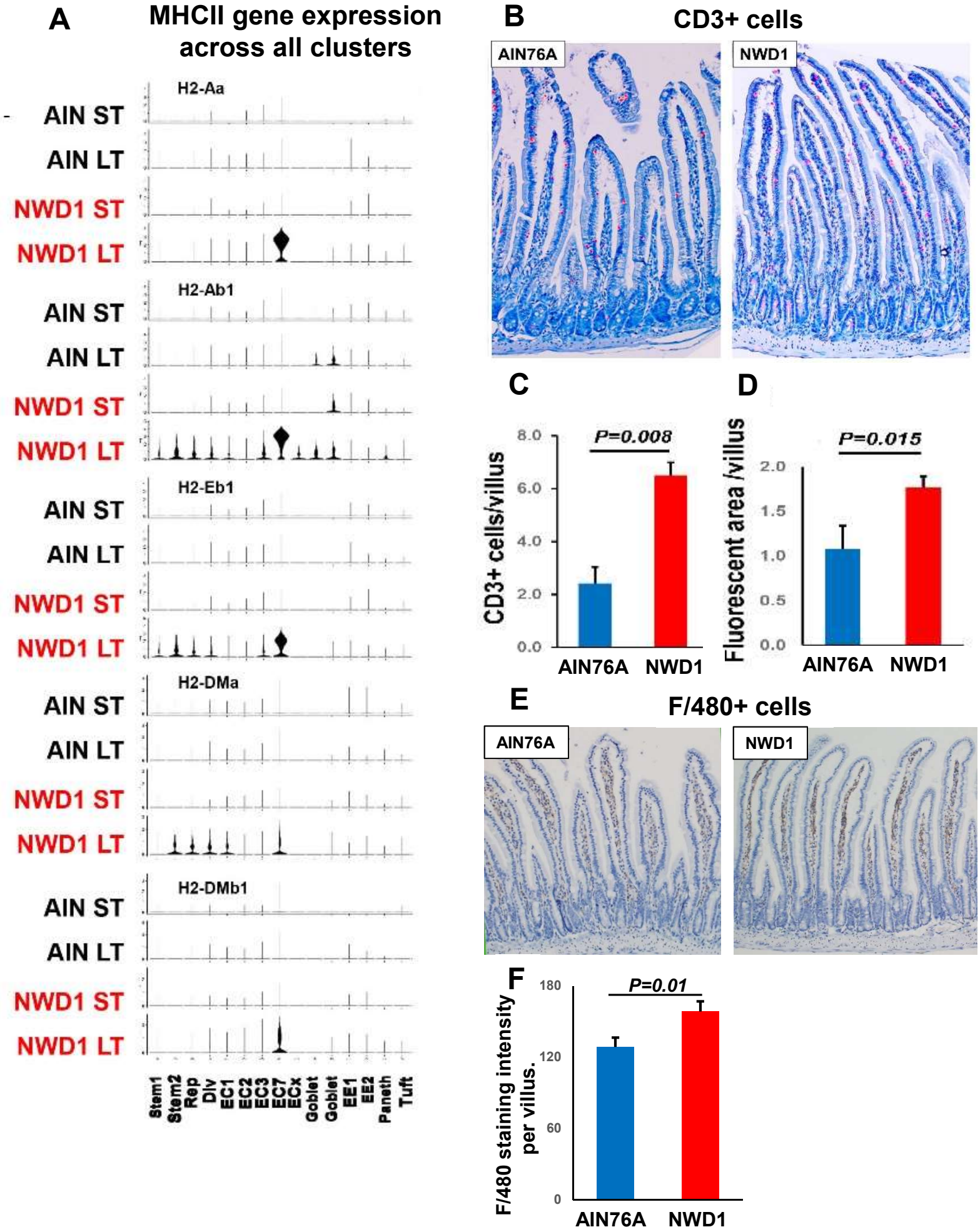
A
MHCII gene expression across all clusters
H2-Aa
H2-Ab1
H2-Eb1
H2-DMa
H2-DMb1
AIN ST
AIN LT
NWD1 ST
NWD1 LT
Stem1
Stem2
Rep
Dlv
EC1
EC2
EC3
EC7
ECx
Goblet
Goblet
EE1
EE2
Paneth
Tuft
B
CD3+ cells
AIN76A
NWD1
C
P=0.008
CD3+ cells/villus
8.0
6.0
4.0
2.0
0.0
AIN76A
NWD1
D
P=0.015
Fluorescent area /villus
2.0
1.5
1.0
0.5
0.0
AIN76A
NWD1
E
F/480+ cells
AIN76A
NWD1
F
P=0.01
F/480 staining intensity per villus.
180
120
60
0
AIN76A
NWD1

<u>Figure 13</u>: An underlying inflammatory response to NWD1: A, expression of 5 genes encoding proteins of the MHCII pathway across cell type/lineages in relation to diet and shorter term (ST= 3d) or longer term (LT=66-70d) post Tam marking of Bmi1+ cells; **B**, immuno-histochemical detection of CD3+ cells in AIN76A and NWD1 fed mice; quantitation of CD3+ cells in relation to diet by number of CD3+/villus (**C**) or area of red fluorescent staining in the mucosa (**D**), N=3 mice per dietary group; **E**, F480+ cells in AIN76A and NWD1 fed mice; **F**, staining intensity per villus, N=3 mice per dietary group.

Fig 14

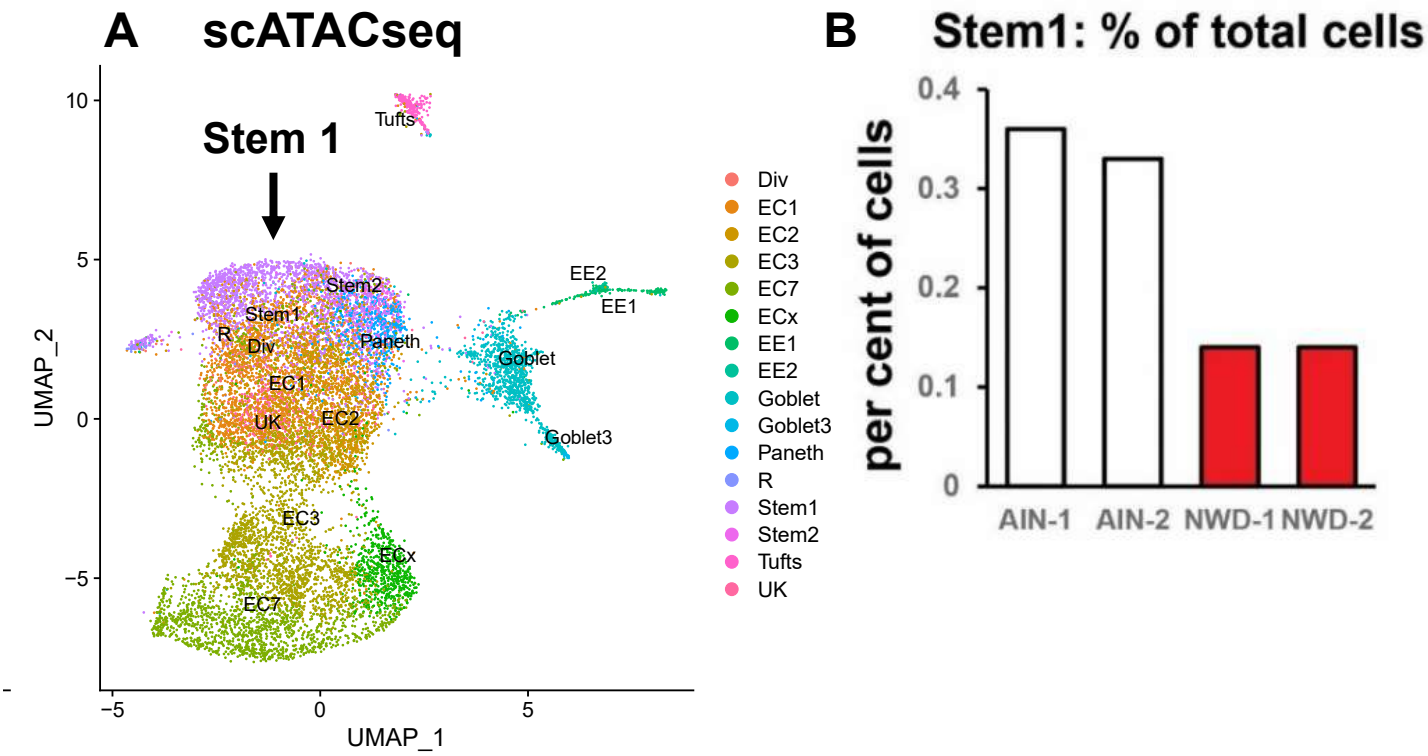
A scATACseq
Stem 1
Tufts
Stem2
Stem1
R
Div
Paneth
EC1
UK
EC2
EE2
EE1
Goblet
Goblet3
EC3
ECx
EC7
UMAP_2
UMAP_1
10
5
0
−5
Div
EC1
EC2
EC3
EC7
ECx
EE1
EE2
Goblet
Goblet3
Paneth
R
Stem1
Stem2
Tufts
UK
B Stem1: % of total cells
per cent of cells
0.4
0.3
0.2
0.1
0
AIN-1
AIN-2
NWD-1
NWD-2

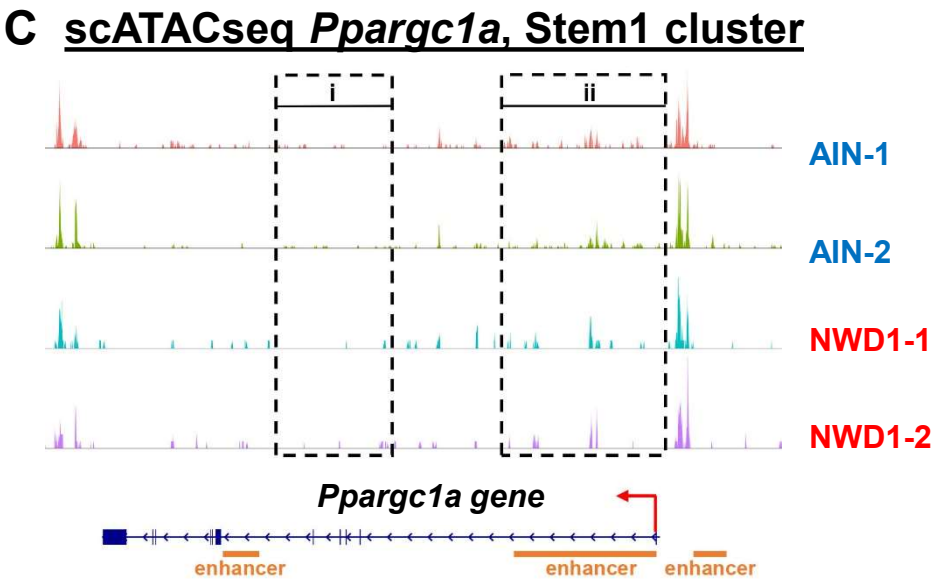
C scATACseq *Ppargc1a*, Stem1 cluster
i
ii
AIN-1
AIN-2
NWD1-1
NWD1-2
Ppargc1a gene
enhancer
enhancer
enhancer

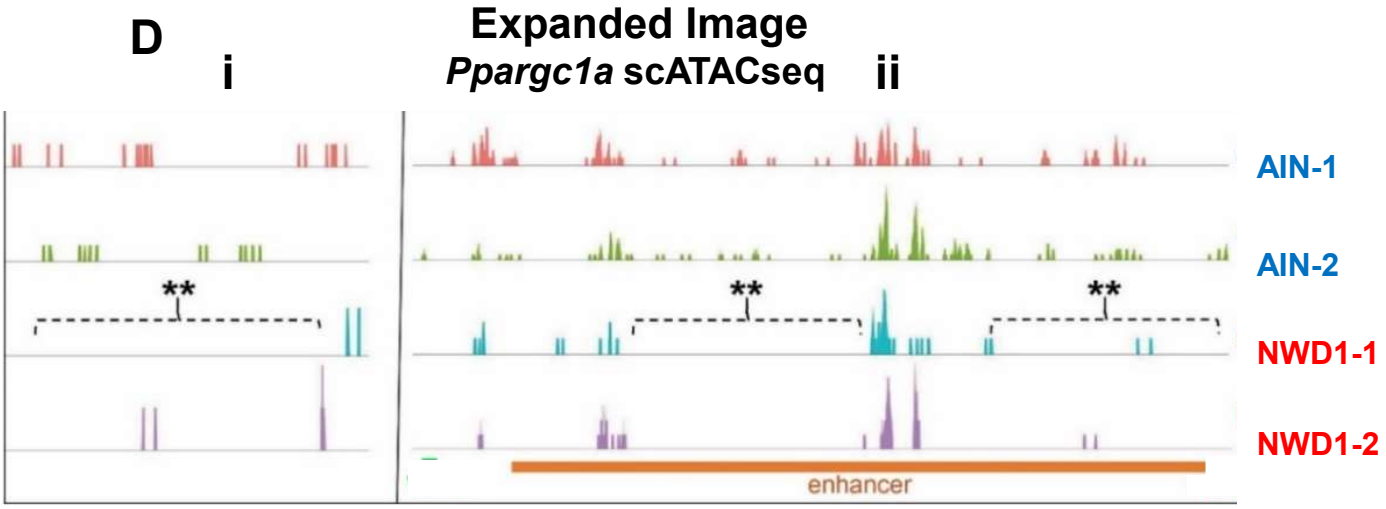
D
Expanded Image
Ppargc1a scATACseq
i
ii
AIN-1
AIN-2
NWD1-1
NWD1-2
**
**
**
enhancer

<u>Figure 14</u>: single cell ATAC seq data, stem cells: Wild-type mice were fed AIN76A or NWD1 for 4 months, then nuclei from total intestinal Epcam+, CD45 negative epithelial cells isolated by FACS were analyzed by single cell ATACseq. **A,** cell types and lineages identified by scATACseq; **B**, per cent Stem 1 cells in mice fed AIN76A or NWD1 based on the scATACseq data; **C,** scATACseq data for the *Ppargc1a* gene in the Stem 1 cluster; **D,** regions i and ii in C enlarged: starred brackets denote regions in which open chromatin structure in AIN76A control fed mice show no signal in NWD1 fed mice.

Fig 15

A **scATACseq *Trpv6*, Ec cluster**

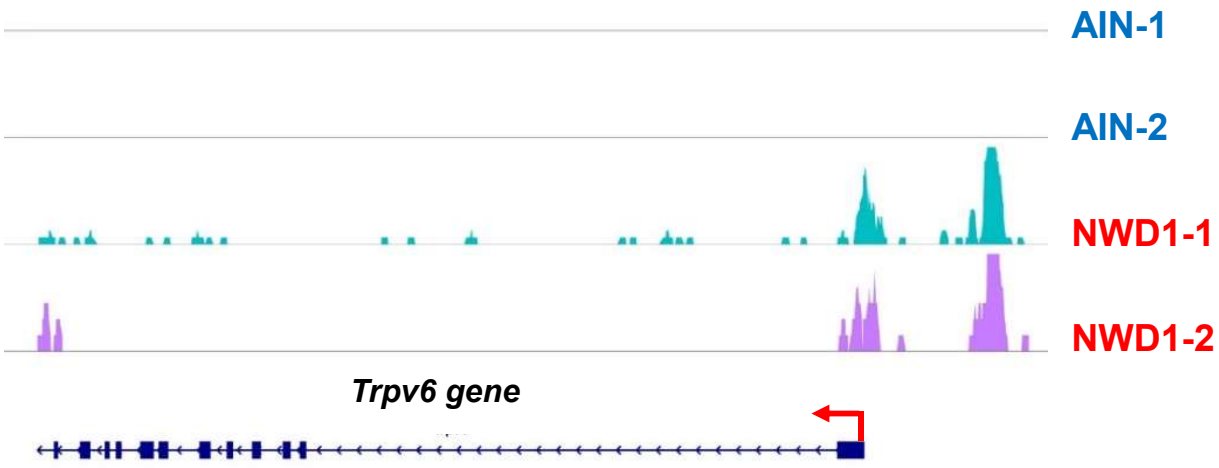

B **scATACseq *Cyp4a10*, Ec cluster**

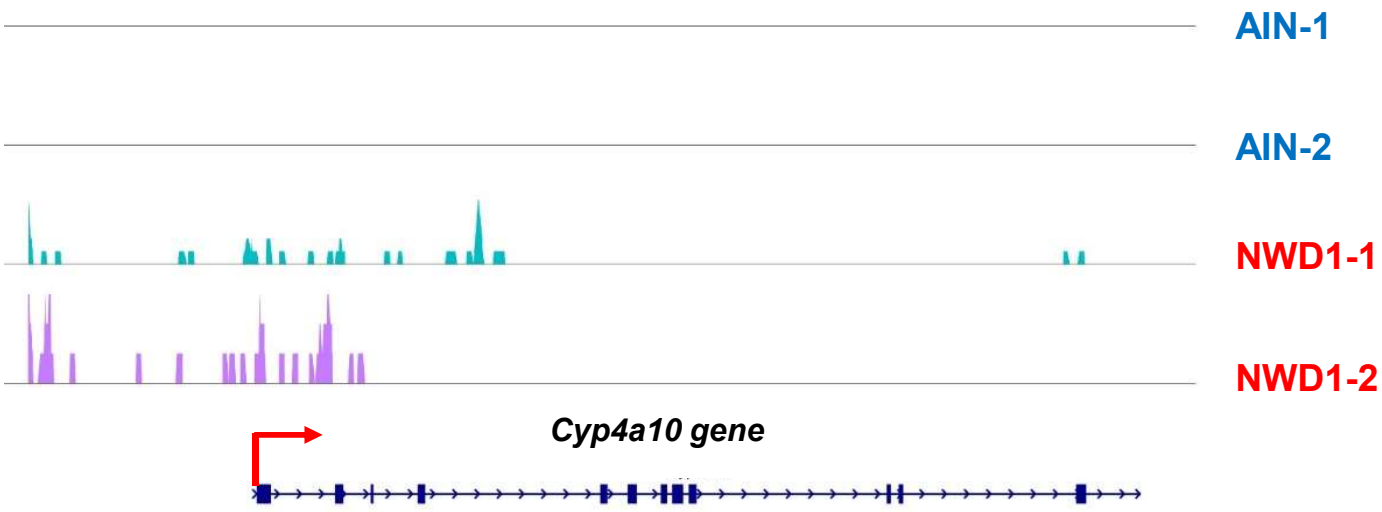

Figure 15: **A,** scATACseq data for the *Trpv6* gene in cells of cluster Ecx for mice fed AIN76A or NWD1; **B,** scATACseq data for the *Cyp4a10* gene in Ecx cluster for mice fed AIN76A or NWD1

Table S1: All pathways significantly altered in Lgr5^{hi} cells of NWD1 fed mice

Pathway	3 months NES	3 months P value	3 months FDR	12 months NES	12 months P value	12 months FDR	NWD1/AIN cross-over NES	NWD1/AIN cross-over P value	NWD1/AIN cross-over FDR
_RIBOSOME	3.190	≤0.001	0.000	3.100	≤0.001	0.000	-3.130	≤0.001	0.000
_DNA_REPLICATION	2.410	≤0.001	0.000	2.260	≤0.001	0.000	-2.470	≤0.001	0.000
_SPLICEOSOME	2.340	≤0.001	0.000	2.080	≤0.001	0.000	-2.340	≤0.001	0.000
_RNA_POLYMERASE	2.190	≤0.001	0.000	1.880	≤0.001	0.001	-2.000	≤0.001	0.001
_MISMATCH_REPAIR	2.130	≤0.001	0.000	2.140	≤0.001	0.000	-2.210	≤0.001	0.000
_CELL_CYCLE	1.970	≤0.001	0.001	1.910	≤0.001	0.001	-2.080	≤0.001	0.000
_NUCLEOTIDE_EXCISION_REPAIR	1.830	≤0.001	0.006	1.900	≤0.001	0.001	-1.780	0.003	0.009
_TASTE_TRANSDUCTION	1.780	≤0.001	0.011						
_PURINE_METABOLISM	1.740	≤0.001	0.015	1.600	≤0.001	0.038	-1.540	0.002	0.079
_OOCYTE_MEIOSIS	1.730	0.002	0.016	1.420	0.030	0.160	-1.260	0.091	0.333
_PYRIMIDINE_METABOLISM	1.720	≤0.001	0.015	1.800	≤0.001	0.003	-1.670	≤0.001	0.026
_BASE_EXCISION_REPAIR	1.680	0.004	0.020	2.090	≤0.001	0.000	-1.990	≤0.001	0.001
_RNA_DEGRADATION	1.680	≤0.001	0.019	1.630	0.006	0.031	-1.360	0.078	0.213
_LINOLEIC_ACID_METABOLISM	1.660	0.004	0.020	1.460	0.062	0.153			
_ARACHIDONIC_ACID_METABOLISM	1.590	0.015	0.038						
_WNT_SIGNALING_PATHWAY	1.520	≤0.001	0.063						
_ALPHA_LINOLENIC_ACID_METABOLISM	1.490	0.042	0.072	1.400	0.068	0.189			
_DORSO_VENTRAL_AXIS_FORMATION	1.470	0.047	0.082						
_PROGESTERONE_MEDIATED_OOCYTE_MATURATION	1.450	0.021	0.088	1.440	0.018	0.157			
_ETHER_LIPID_METABOLISM	1.410	0.072	0.116						
_AMINOACYL_TRNA_BIOSYNTHESIS				1.440	0.047	0.149	-1.530	0.031	0.073
_HOMOLOGOUS_RECOMBINATION				1.960	≤0.001	0.001	-2.430	≤0.001	0.000
_BASAL_CELL_CARCINOMA				1.460	0.034	0.160	-1.360	0.078	0.217
_NOTCH_SIGNALING_PATHWAY				1.450	0.030	0.160			
_BASAL_TRANSCRIPTION_FACTORS				1.390	0.072	0.187	-1.210	0.209	0.388

Pathway	NES	P value	FDR	NES	P value	FDR	NES	P value	FDR
_ABC_TRANSPORTERS	-2.340	≤0.001	≤0.001	-1.980	≤0.001	0.006	1.850	≤0.001	0.010
_CITRATE_CYCLE_TCA_CYCLE	-2.280	≤0.001	≤0.001	-2.020	≤0.001	0.006	2.010	≤0.001	0.002
_PEROXISOME	-2.200	≤0.001	≤0.001		≤0.001			≤0.001	≤0.001
_OXIDATIVE_PHOSPHORYLATION	-2.190	≤0.001	≤0.001	-2.370	≤0.001	≤0.001	2.110	≤0.001	0.001
_PARKINSONS_DISEASE	-2.140	≤0.001	≤0.001	-2.120	≤0.001	0.002	1.930	≤0.001	0.004
_PPAR_SIGNALING_PATHWAY	-2.100	≤0.001	≤0.001		≤0.001				
_FATTY_ACID_METABOLISM	-2.080	≤0.001	≤0.001		≤0.001				
_GLYCOLYSIS_GLUCONEOGENESIS	-2.070	≤0.001	≤0.001	-2.030	≤0.001	0.005			
_RETINOL_METABOLISM	-2.070	≤0.001	≤0.001		≤0.001				
_ALZHEIMERS_DISEASE	-2.020	≤0.001	≤0.001	-2.170	≤0.001	≤0.001	1.950	≤0.001	0.004
_FRUCTOSE_AND_MANNOSE_METABOLISM	-1.980	≤0.001	≤0.001	-2.320	≤0.001	≤0.001	2.280	≤0.001	≤0.001
_ENDOCYTOSIS	-1.980	≤0.001	≤0.001						
_AMINO_SUGAR_AND_NUCLEOTIDE_SUGAR_METABOLISM	-1.920	0.002	0.002				1.720	0.010	0.023
_GLYOXYLATE_AND_DICARBOXYLATE_METABOLISM	-1.850	0.006	0.006						
_INTESTINAL_IMMUNE_NETWORK_FOR_IGA_PRODUCTION	-1.840	0.006	0.006	-1.520	0.049	0.123			
_SPHINGOLIPID_METABOLISM	-1.840	≤0.001	0.006				1.890	0.005	0.008
_BUTANOATE_METABOLISM	-1.820	0.002	0.006						
_EPITHELIAL_CELL_SIGNALING_IN_HELICOBACTER_PYLORI_INFECTION	-1.820	≤0.001	0.007	-1.650	≤0.001	0.070			
_OTHER_GLYCAN_DEGRADATION	-1.800	0.008	0.008	-1.530	0.058	0.133	2.120	≤0.001	≤0.001
_PENTOSE_PHOSPHATE_PATHWAY	-1.780	0.004	0.010	-1.480	0.033	0.138			
_CARDIAC_MUSCLE_CONTRACTION				-1.800	≤0.001	0.028			
_HUNTINGTONS_DISEASE				-1.520	≤0.001	0.127	1.290	0.049	0.203
_SYSTEMIC_LUPUS_ERYTHEMATOSUS					≤0.001				
_STEROID_HORMONE_BIOSYNTHESIS				-2.060	≤0.001	0.004			
_TRYPTOPHAN_METABOLISM				-2.010	≤0.001	0.005			
_RIG_I_LIKE_RECEPTOR_SIGNALING				-1.670	0.012	0.069	1.870	≤0.001	0.009
_DRUG_METABOLISM_CYTOCHROME_P450				-1.580	0.011	0.109	1.330	0.086	0.179
_GALACTOSE_METABOLISM				-1.560	0.051	0.114	1.550	0.029	0.067
_METABOLISM_XENOBIOTICS_BY_CYT_P450				-1.500	0.031	0.131			
_PHOSPHATIDYLINOSITOL_SIGNALING				-1.410	0.026	0.202	1.740	0.005	0.020

Table S1: Pathways significantly altered: GSEA of bulk RNAseq analysis of Lgr5^{hi} cells isolated by FACS from mice fed NWD1 compared to AIN76A for either 3 or 12 months, or for mice fed NWD1 for 3 months than switched back to AIN76A for 9 months, described in Fig 1A.